Electronic Supplementary Material (ESI) for New Journal of Chemistry.

Structure-reactivity relationship of probes based on H_2S-mediated reductive cleavage of C=C bond

Chunfei Wang, Jingyun Tan and Xuanjun Zhang*

Cancer Centre and Centre of Reproduction, Development and Aging, Faculty of Health Sciences, University of Macau, Taipa, Macau SAR, 999078, China. *e-mail: xuanjunzhang@um.edu.mo.

Table of Contents

1. Limit of detection

According to the following Equation, we calculated the limit of detection of **NPTZ-P1** and **NPTZ-P2** to H_2S.

Equation: $C_L=kS_{bi}/m$

Where, m is the slope of the linear regression equation (shown in Figure 3C and 3G). S_{bi} is the standard deviation of the blank measures. Generally, k=3, P<0.01.

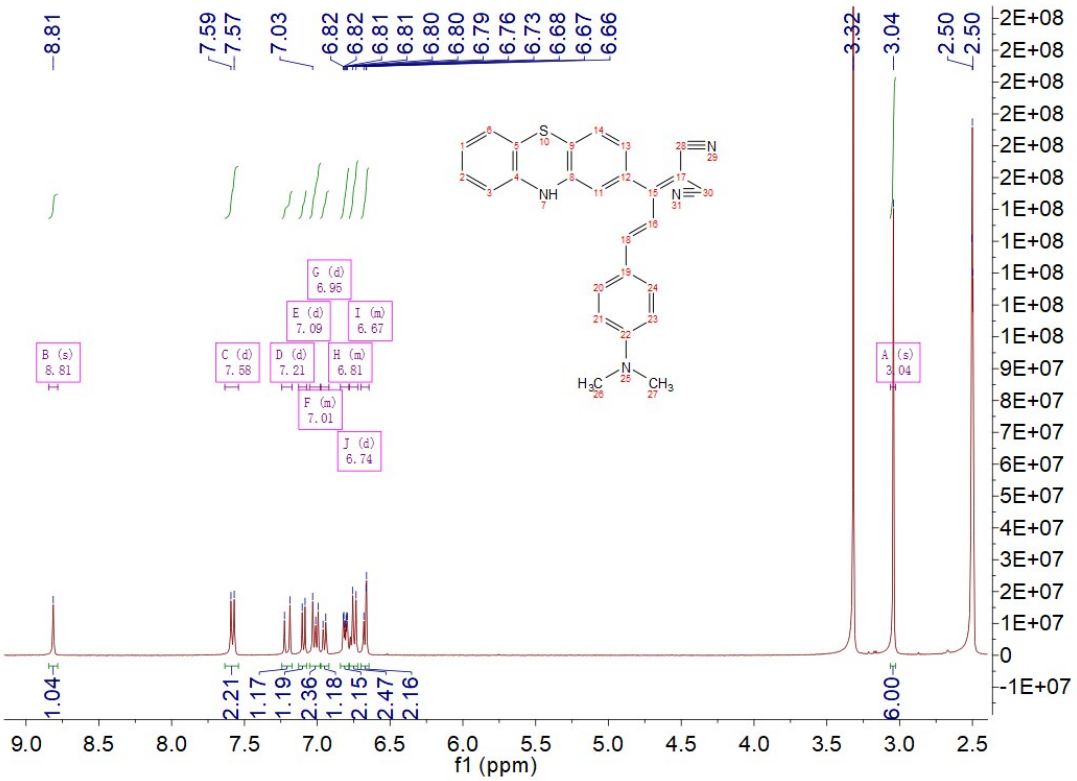

Fig. S1. ^{1}H NMR spectrum of **PTZ-P1** in DMSO.

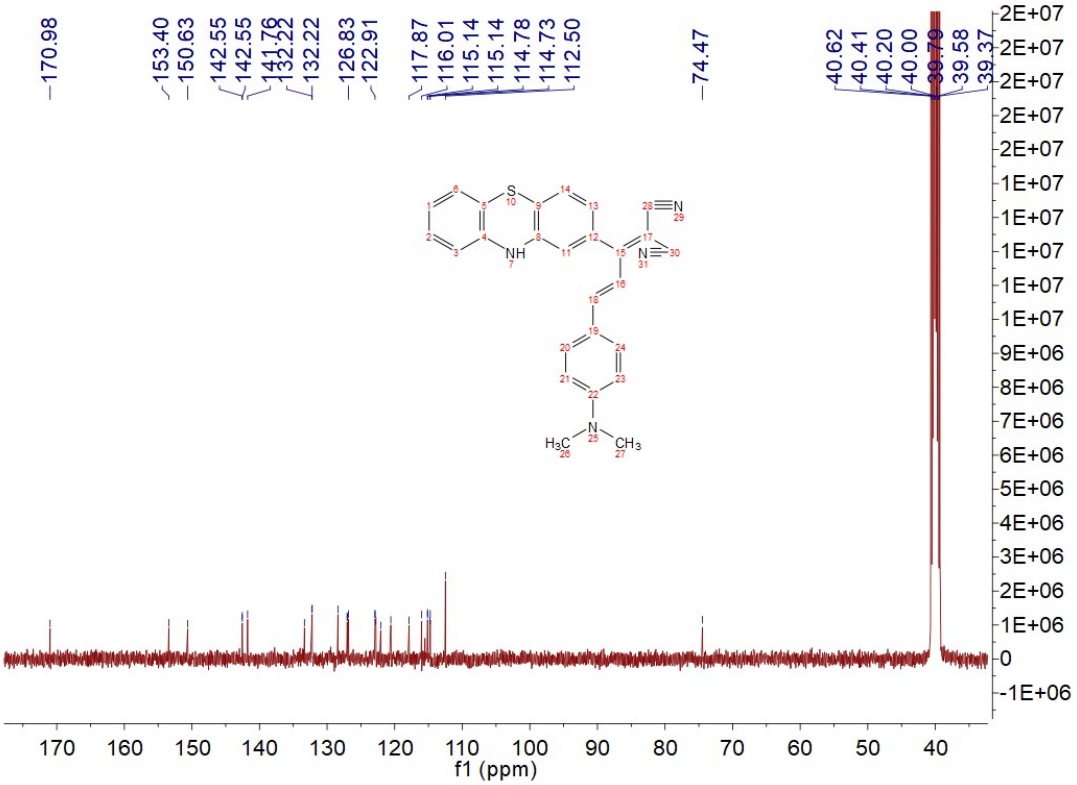

Fig. S2. ^{13}C NMR spectrum of **PTZ-P1** in DMSO.

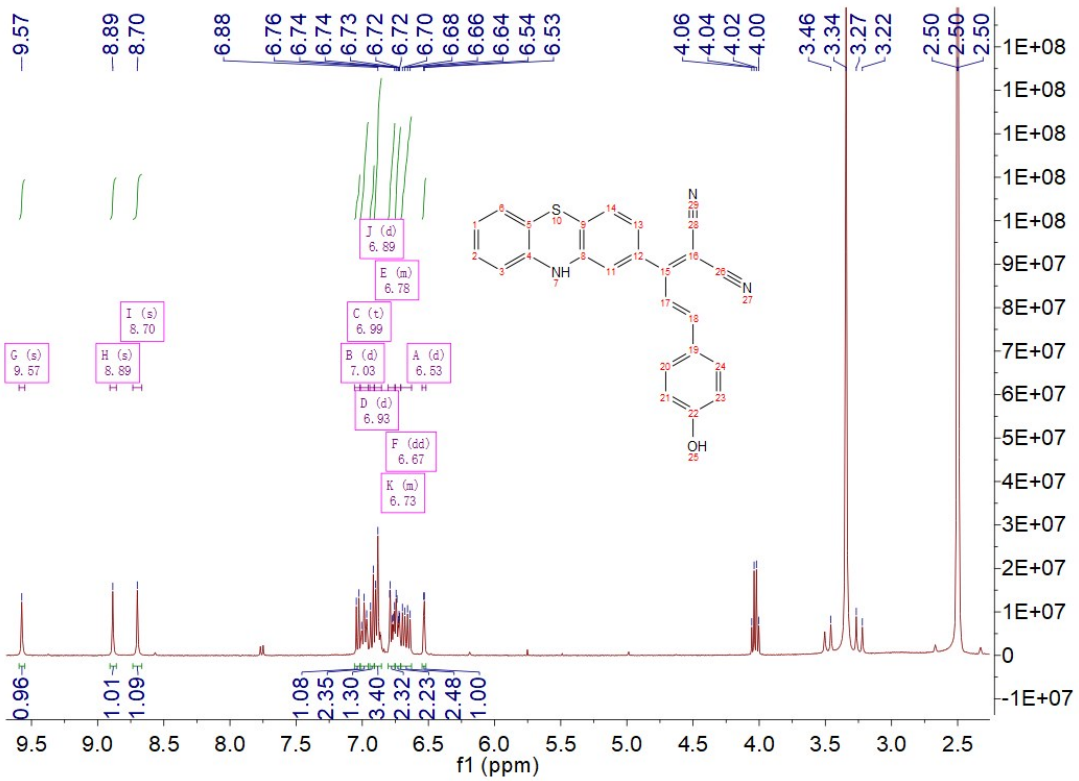

Fig. S3. ^{1}H NMR spectrum of **PTZ-P2** in DMSO.

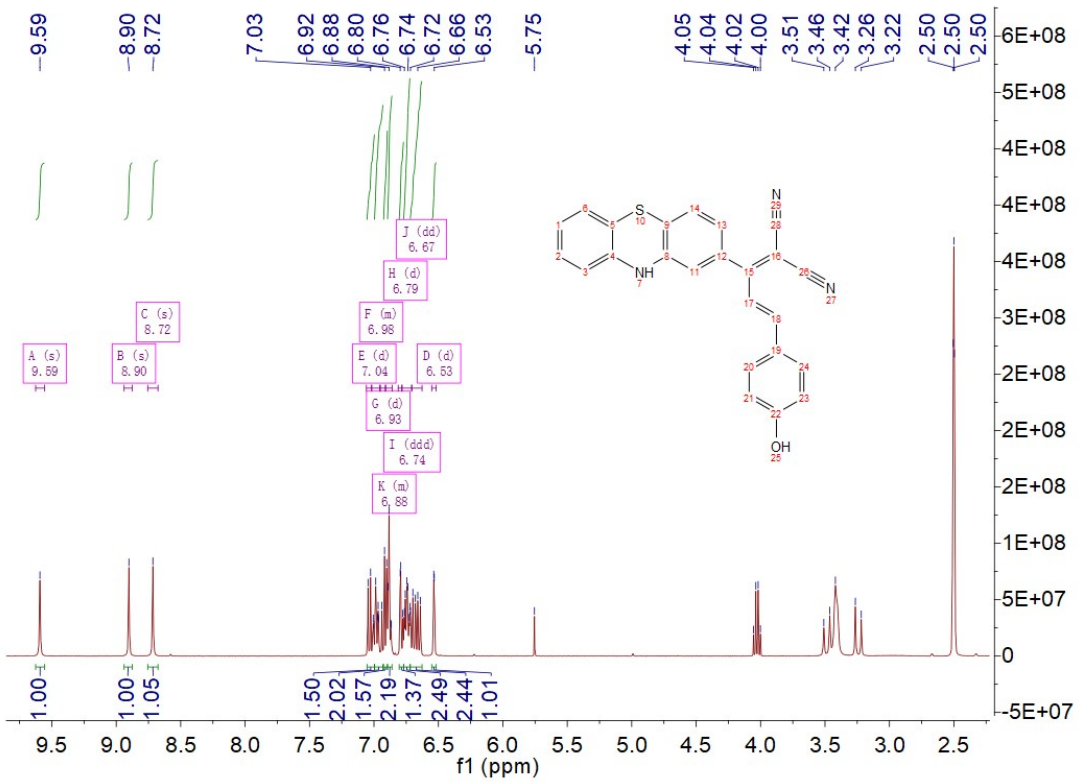

Fig. S4. ^{13}C NMR spectrum of **PTZ-P2** in DMSO.

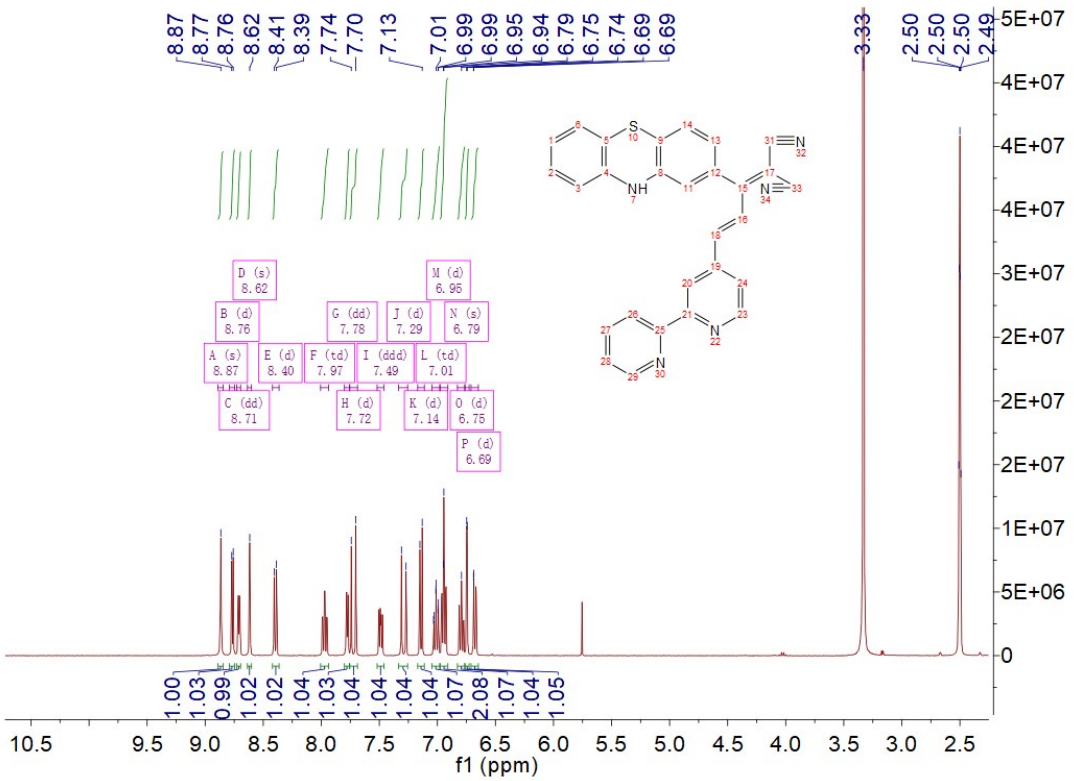

Fig. S5. ^{1}H NMR spectrum of **PTZ-P4** in DMSO.

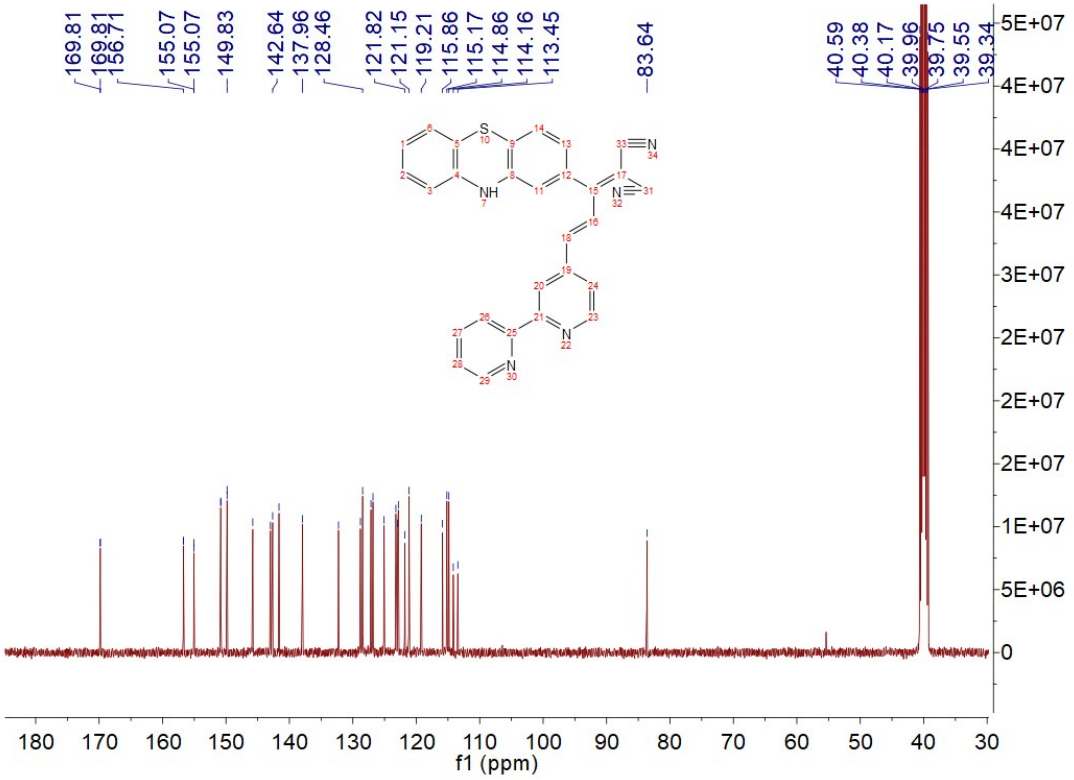

Fig. S6. ^{13}C NMR spectrum of **PTZ-P4** in DMSO.

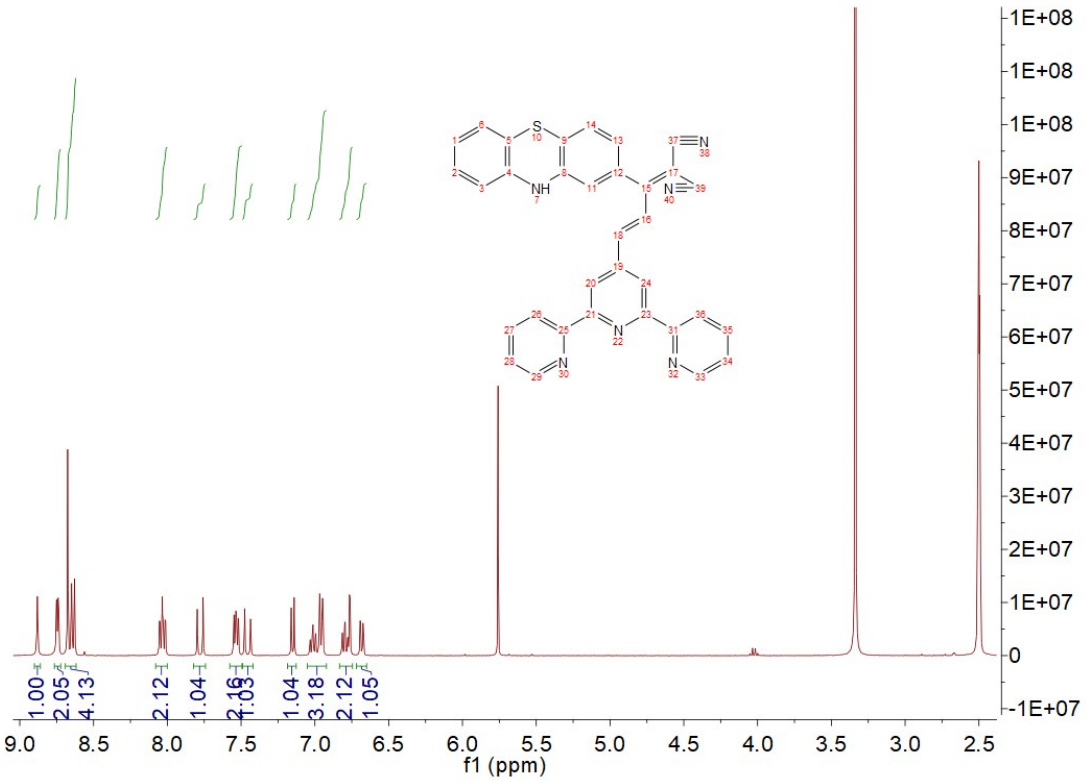

Fig. S7. ^{1}H NMR spectrum of **PTZ-P5** in DMSO.

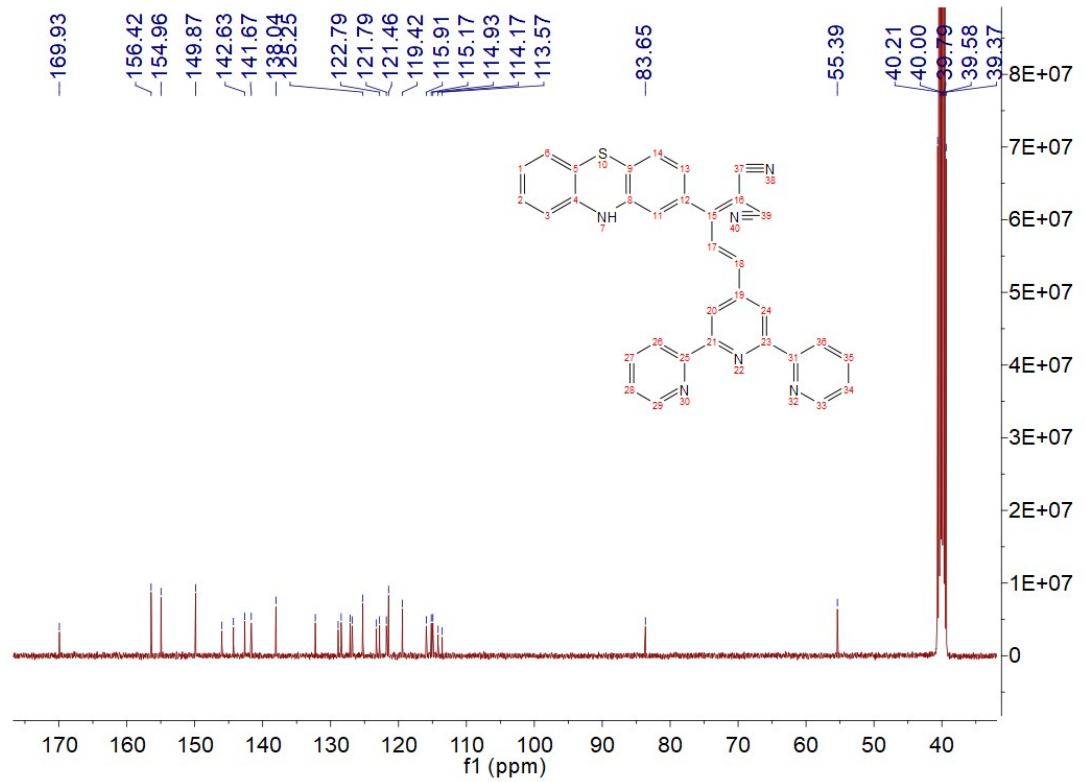

Fig. S8. ^{13}C NMR spectrum of **PTZ-P5** in DMSO.

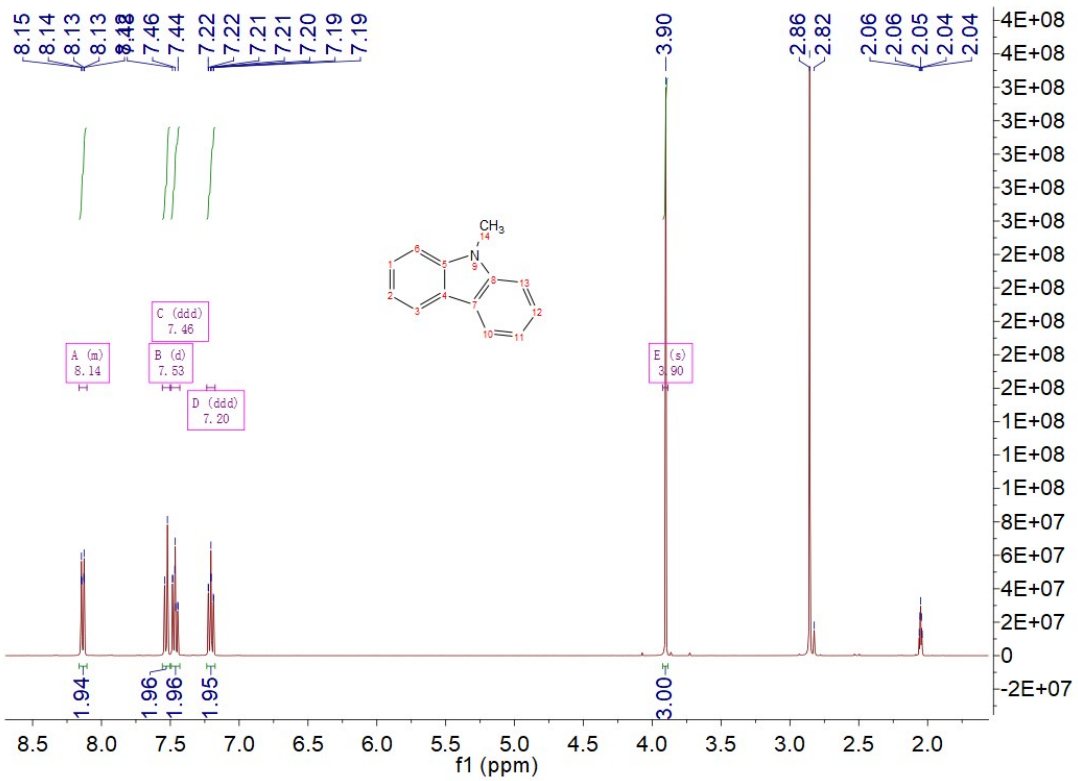

Fig. S9. ^{1}H NMR spectrum of **KZ-1** in $CDCl_3$.

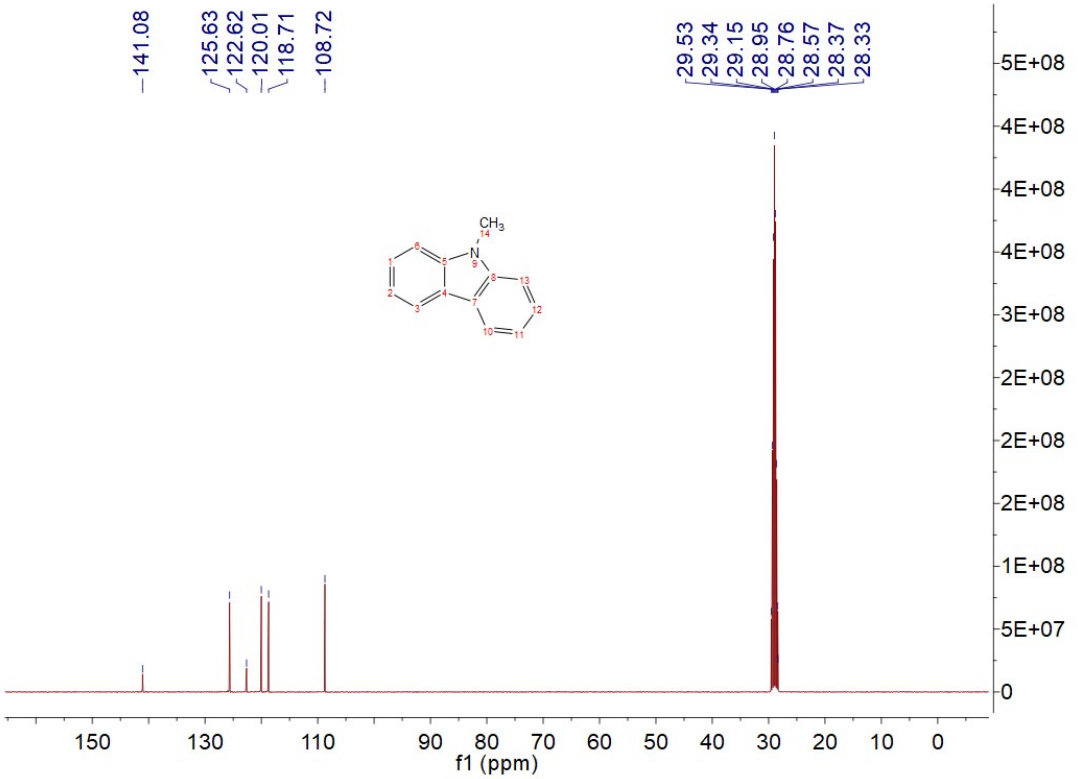

Fig. S10. ^{13}C NMR spectrum of **KZ-1** in $CDCl_3$.

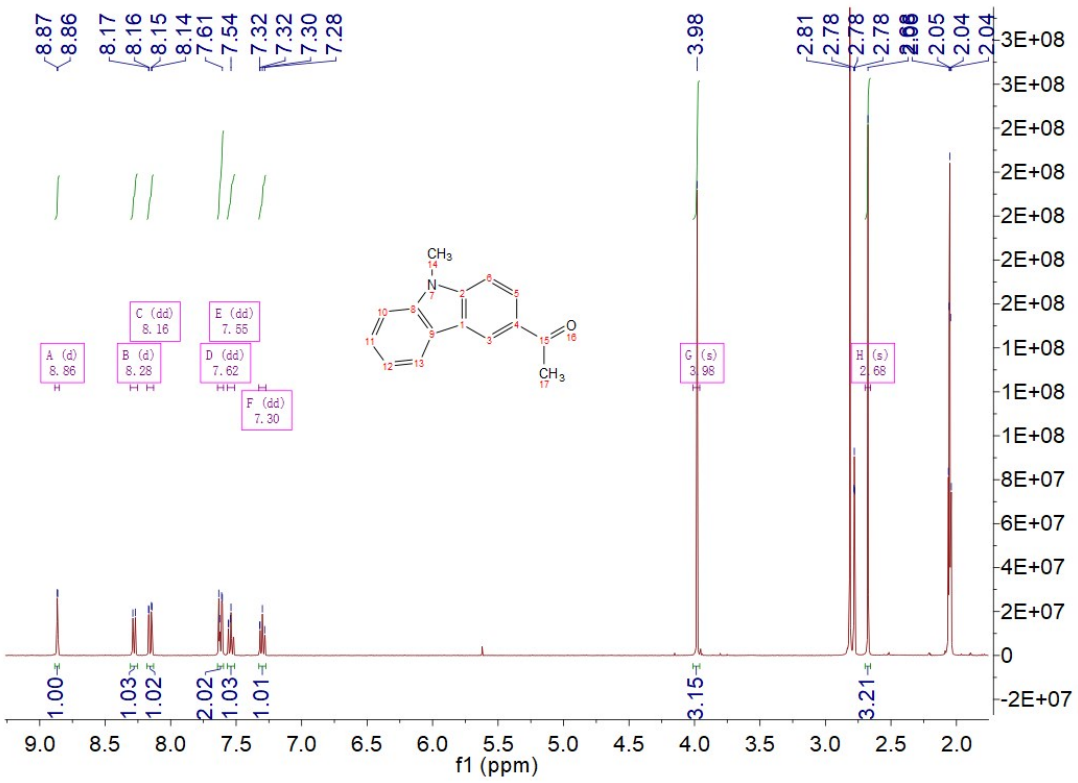

Fig. S11. ^{1}H NMR spectrum of **KZ-2** in Acetone.

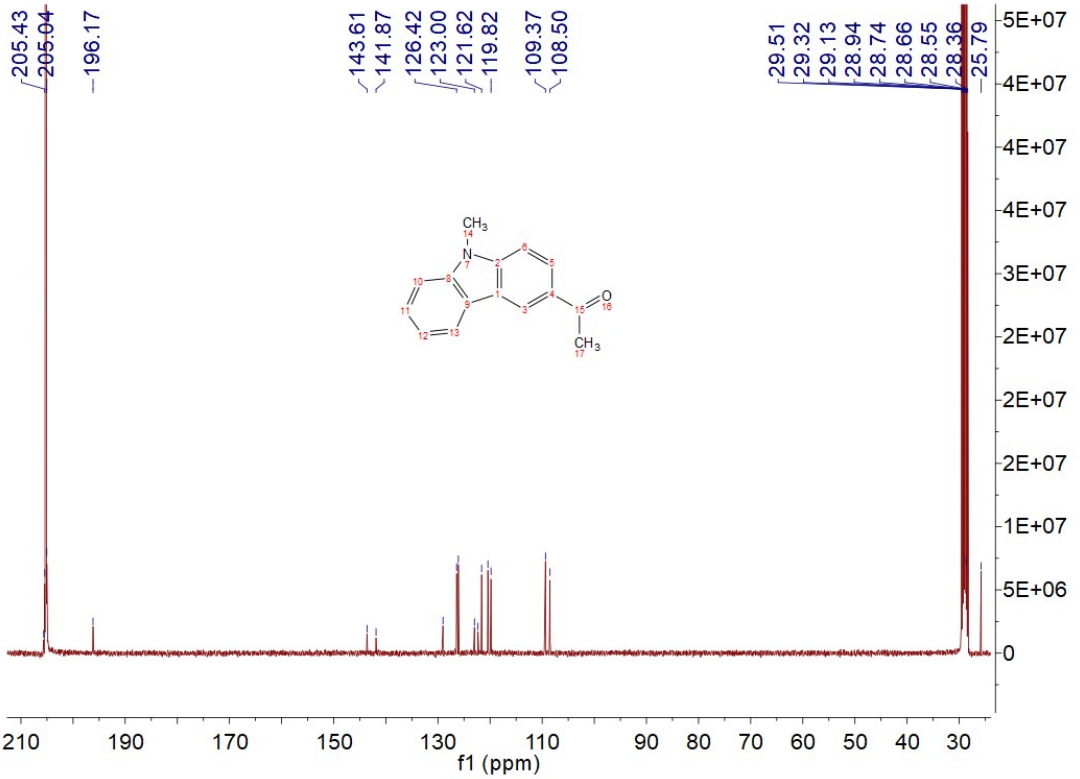

Fig. S12. ^{13}C NMR spectrum of **KZ-2** in Acetone.

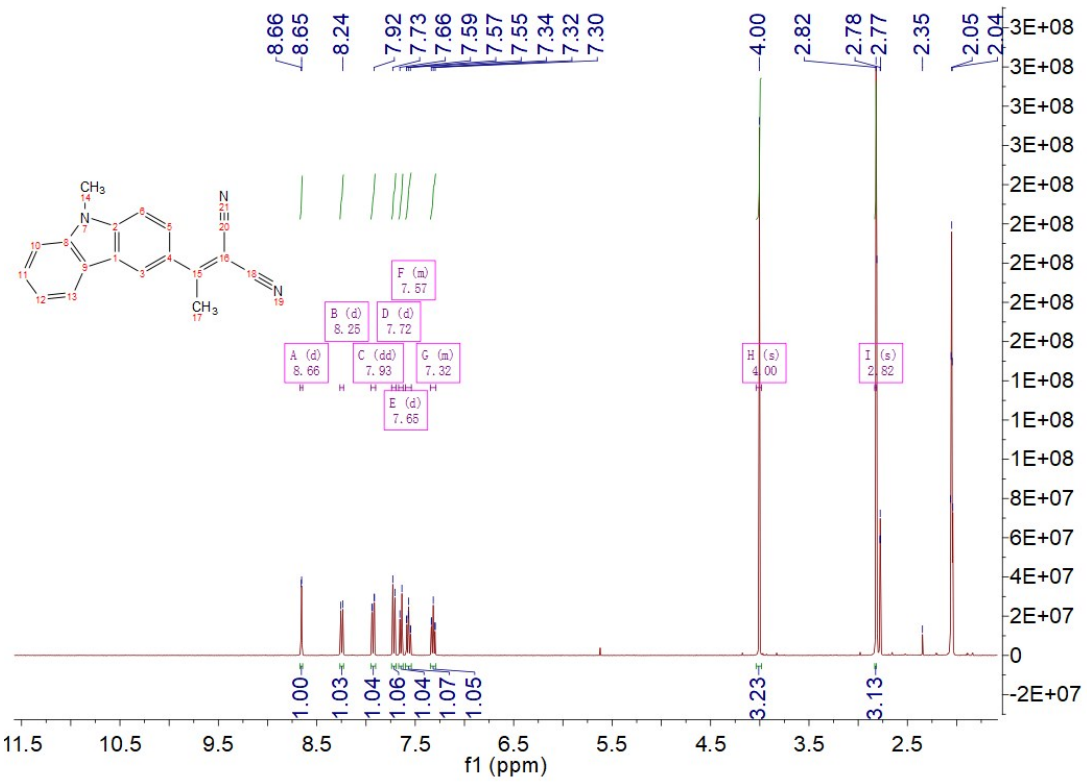

Fig. S13. ^{1}H NMR spectrum of **KZ-3** in Acetone.

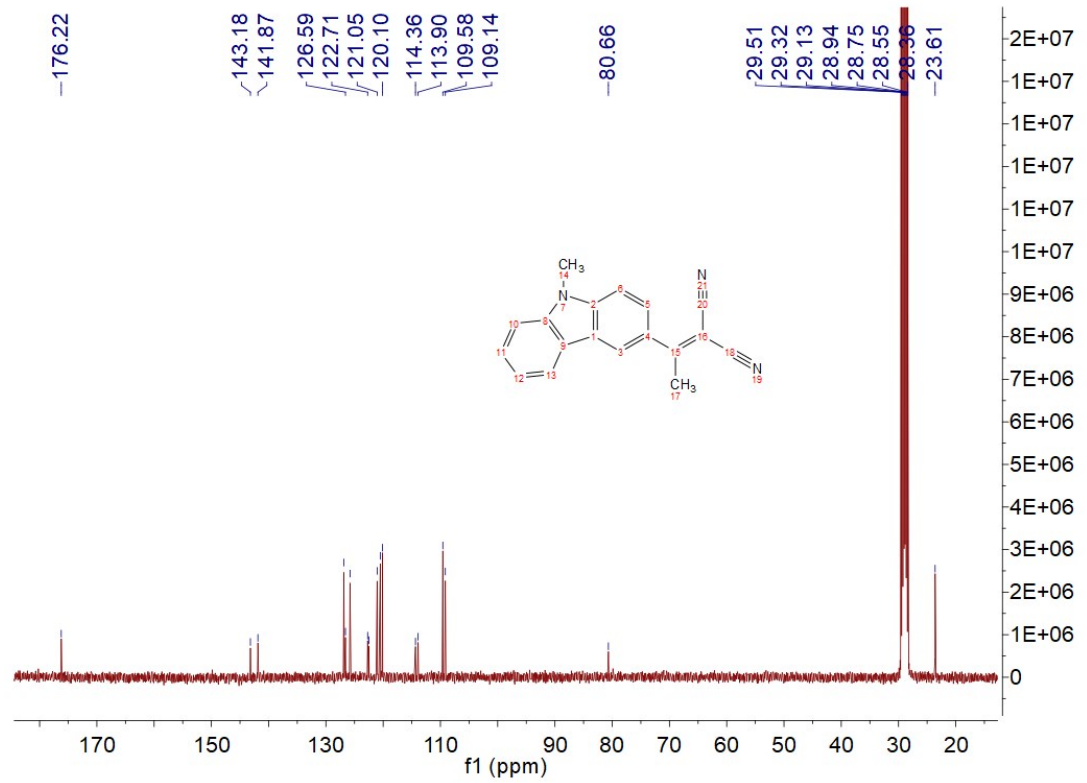

Fig. S14. ^{13}C NMR spectrum of **KZ-3** in Acetone.

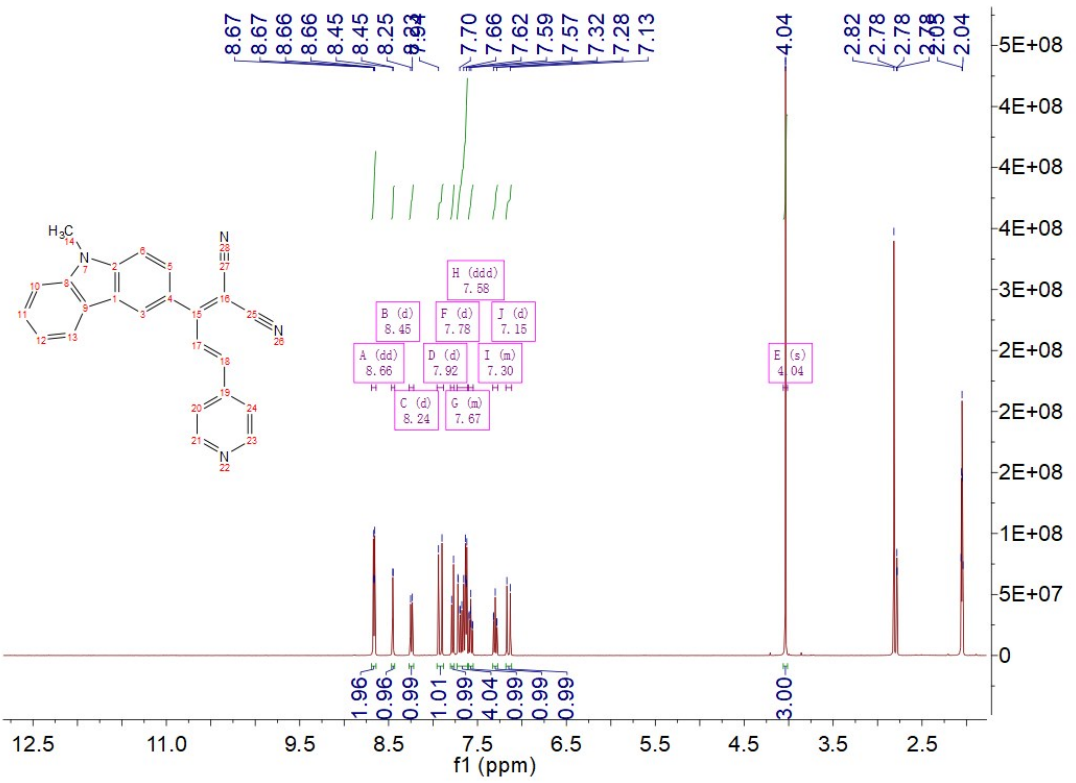

Fig. S15. ^{1}H NMR spectrum of **KZ-P** in Acetone.

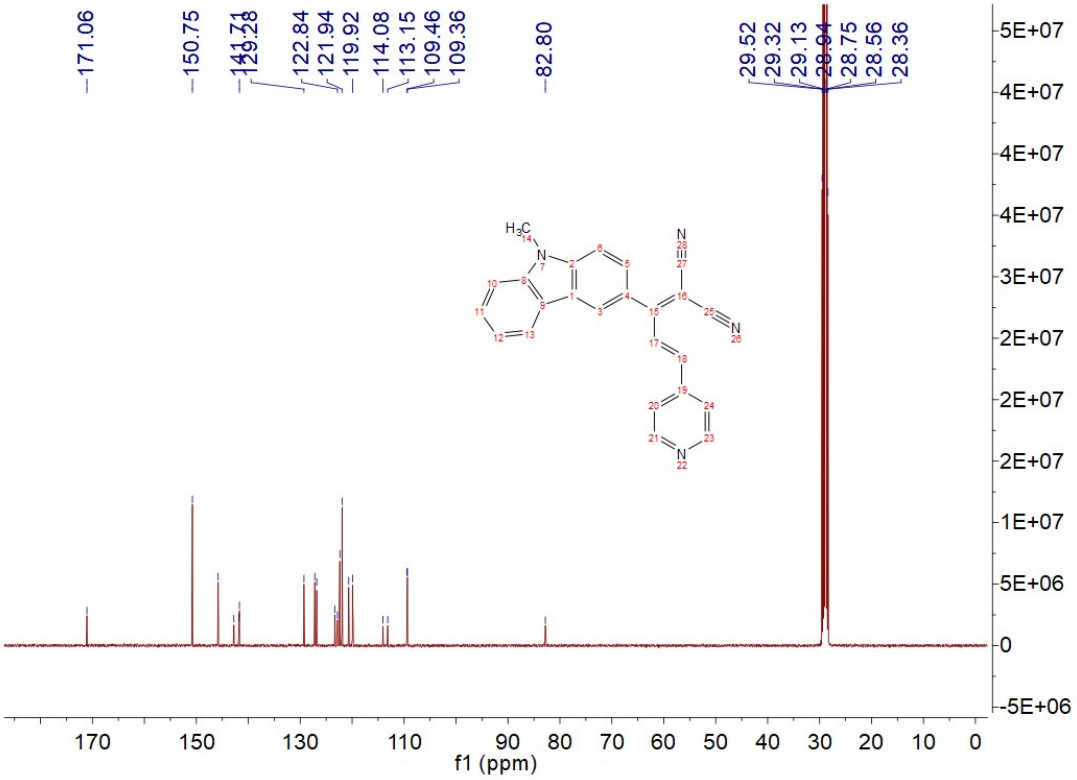

Fig. S16. ^{13}C NMR spectrum of **KZ-P** in Acetone.

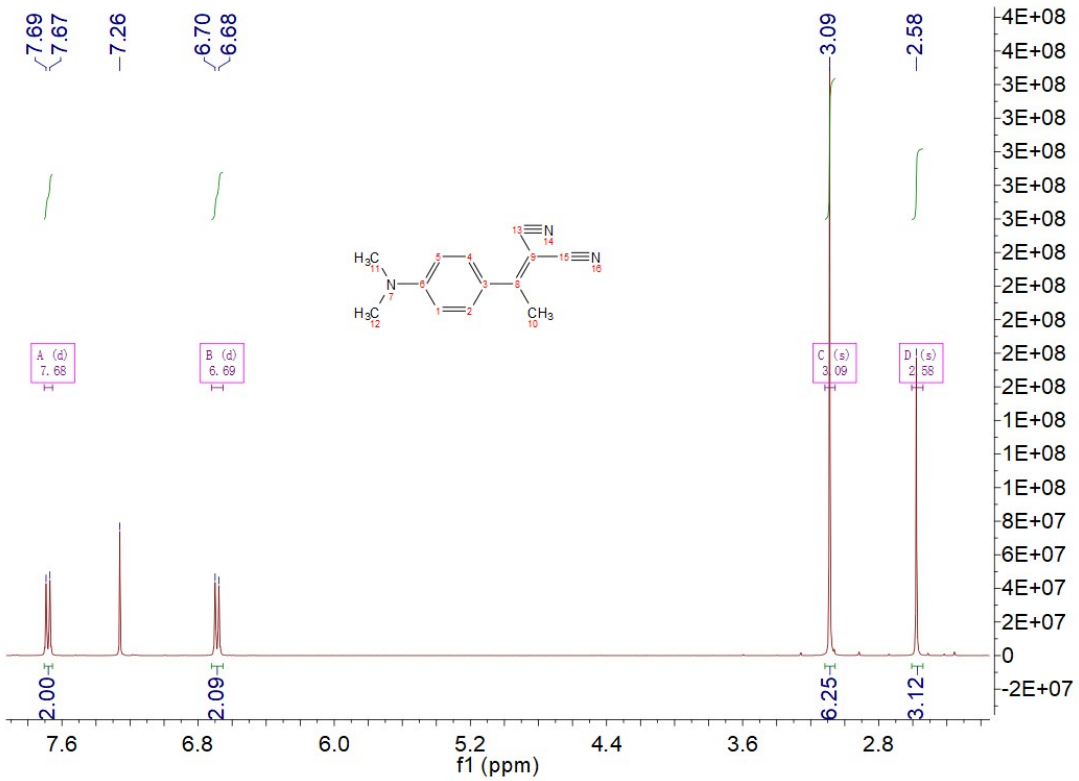

Fig. S17. ^{1}H NMR spectrum of **NNP-1** in $CDCl_3$.

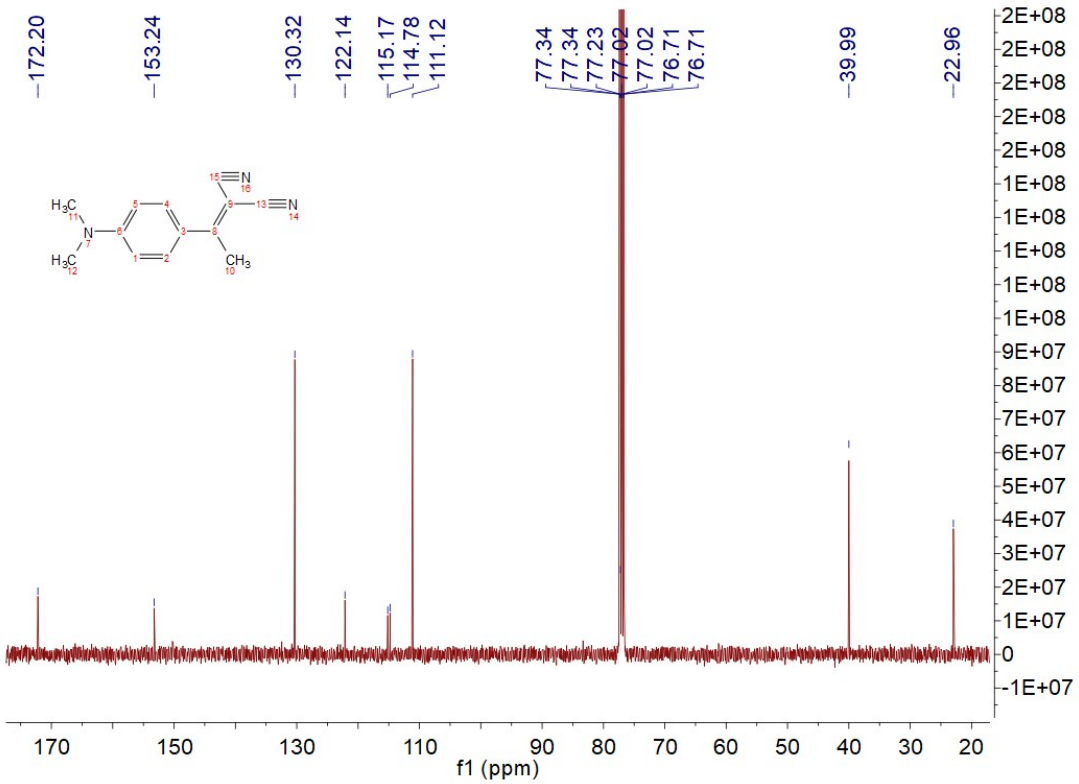

Fig. S18. ^{13}C NMR spectrum of **NNP-1** in $CDCl_3$.

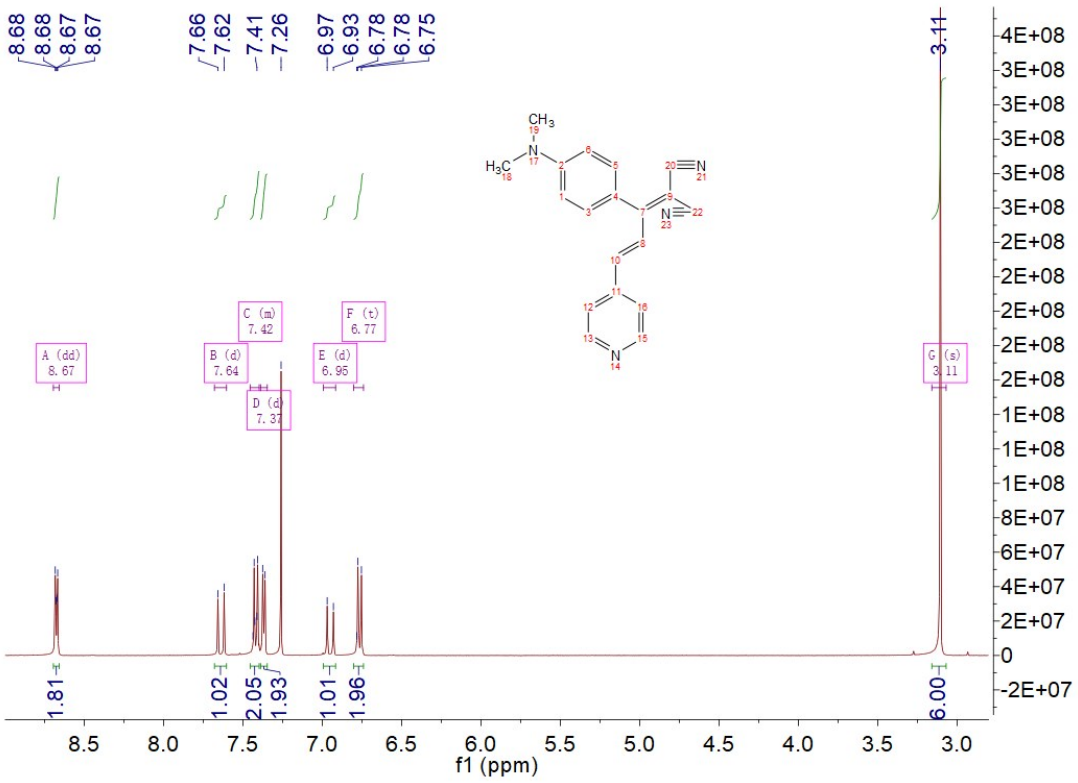

Fig. S19. ^{1}H NMR spectrum of **NNP-P** in $CDCl_3$.

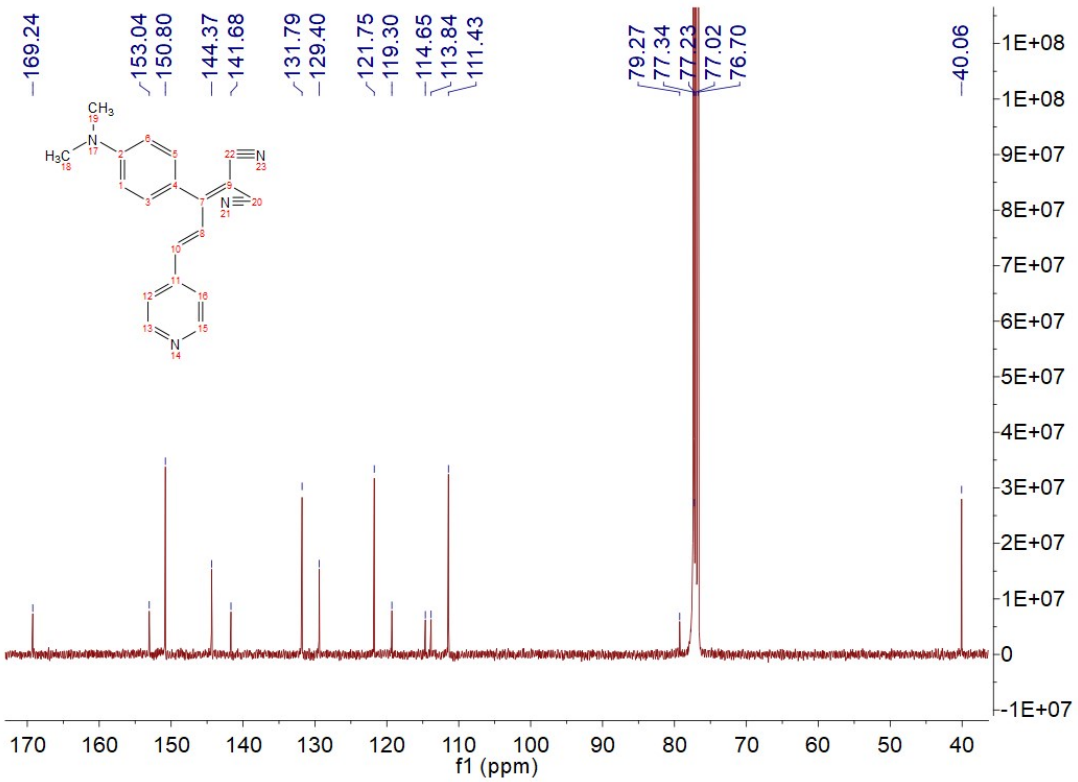

Fig. S20. ^{13}C NMR spectrum of **NNP-P** in $CDCl_3$.

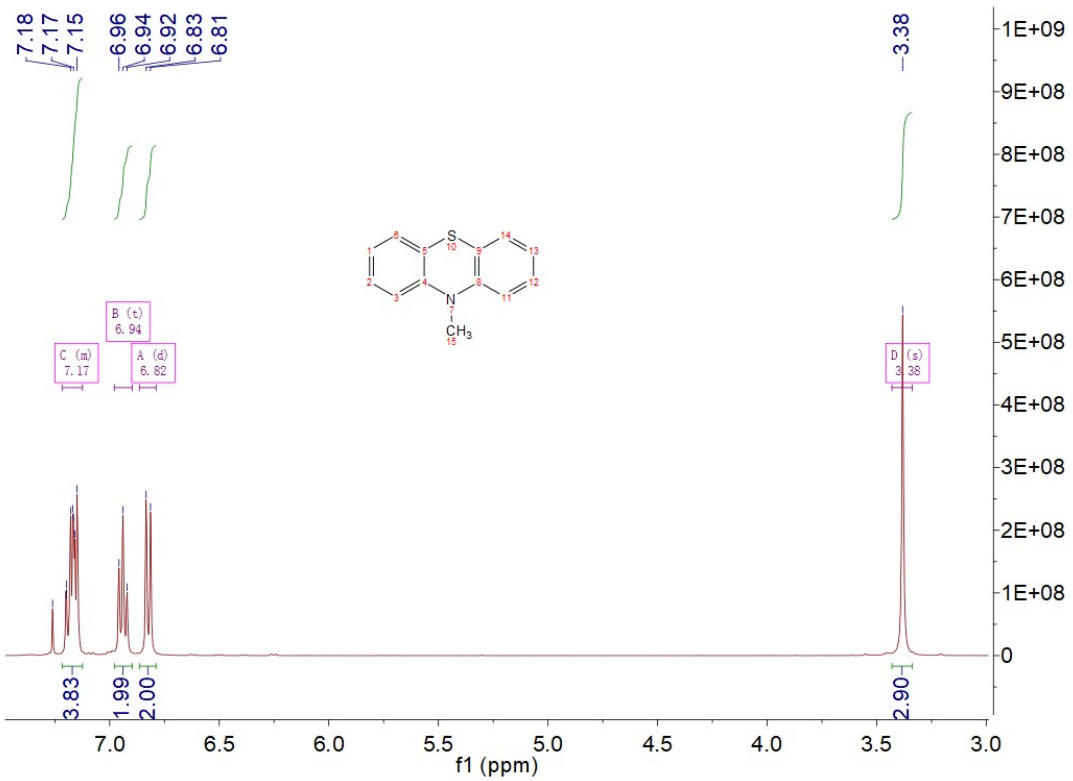

Fig. S21. ^{1}H NMR spectrum of **PTZ-1** in $CDCl_3$.

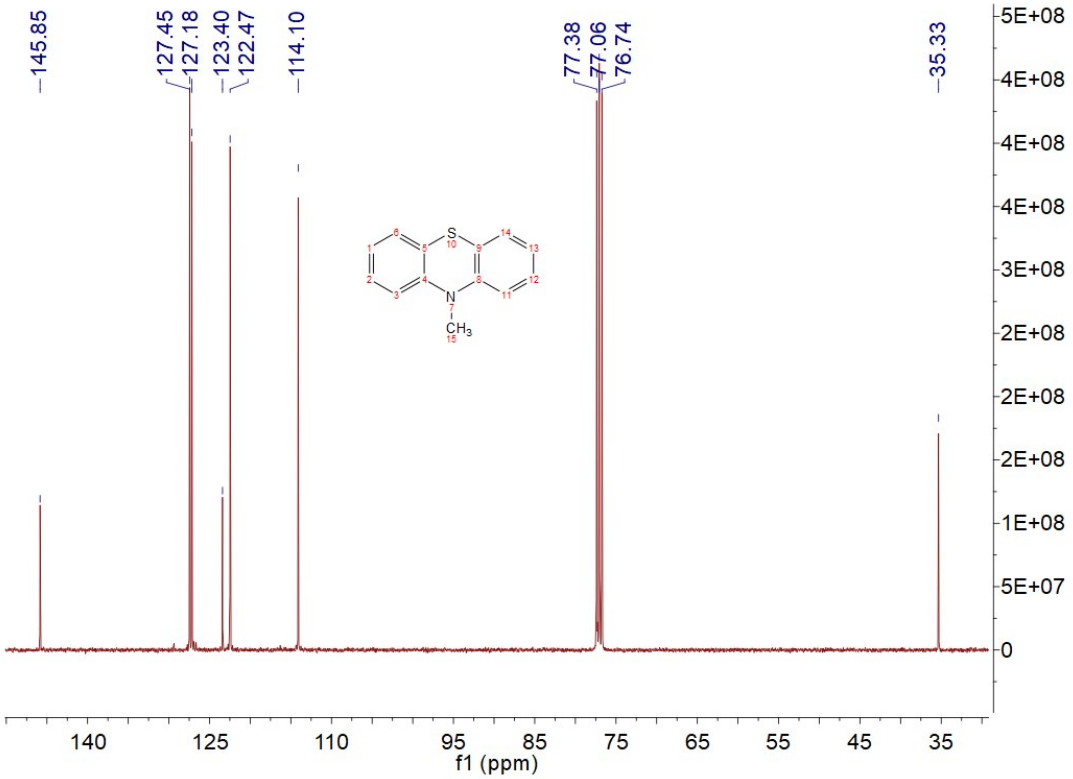

Fig. S22. ^{13}C NMR spectrum of **PTZ-1** in $CDCl_3$.

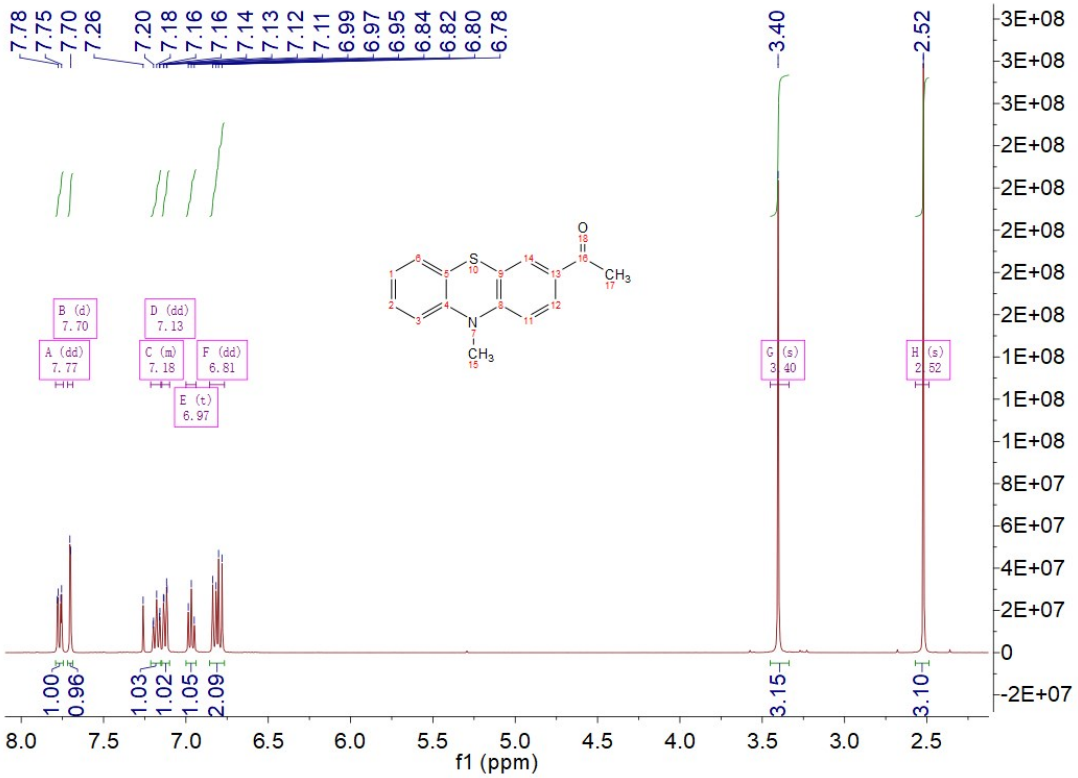

Fig. S23. ^{1}H NMR spectrum of **PTZ-2** in $CDCl_3$.

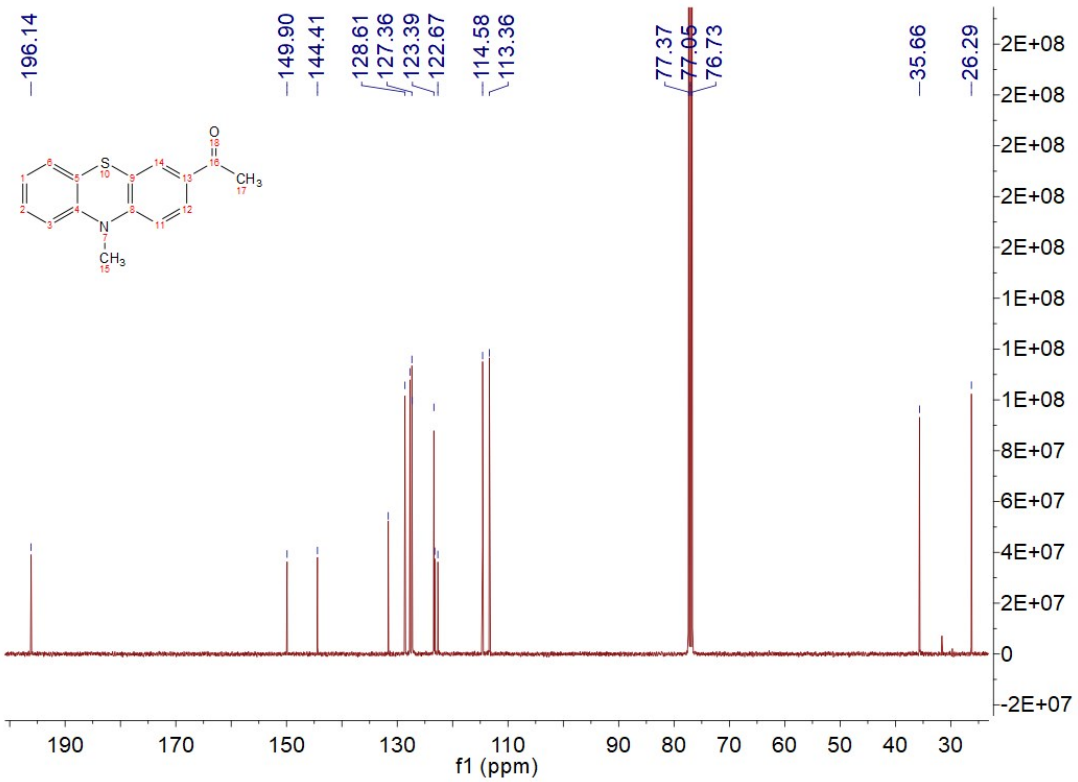

Fig. S24. ^{13}C NMR spectrum of **PTZ-2** in $CDCl_3$.

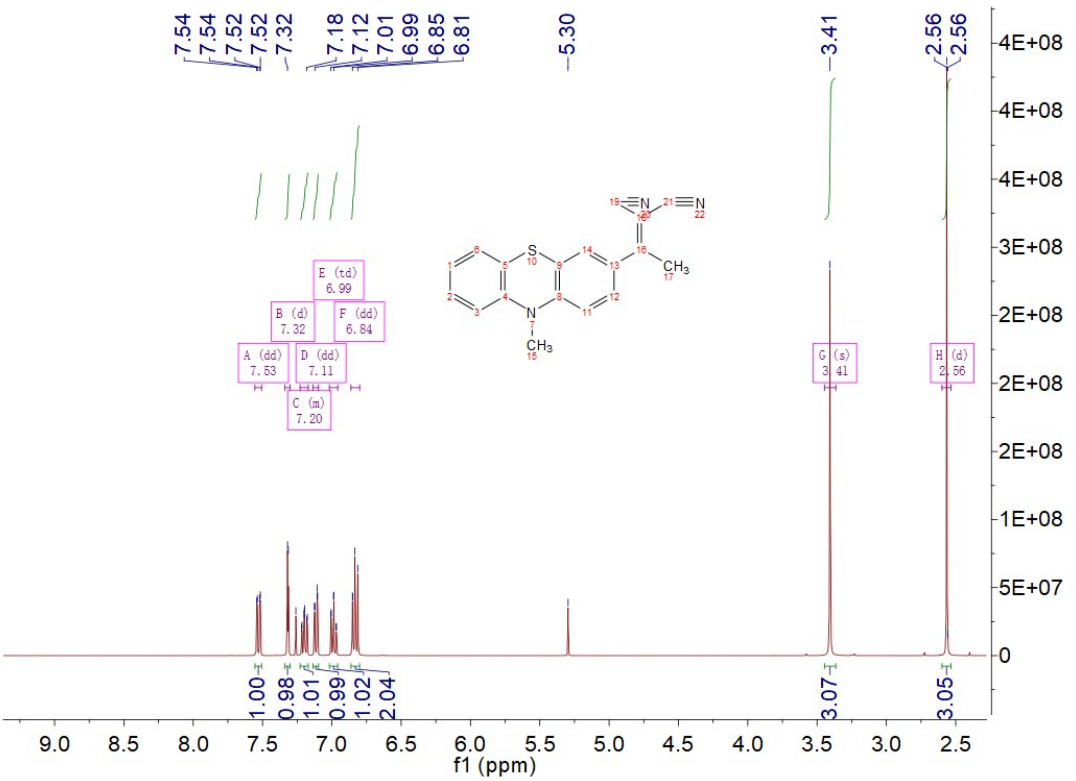

Fig. S25. ^{1}H NMR spectrum of **PTZ-3** in $CDCl_3$.

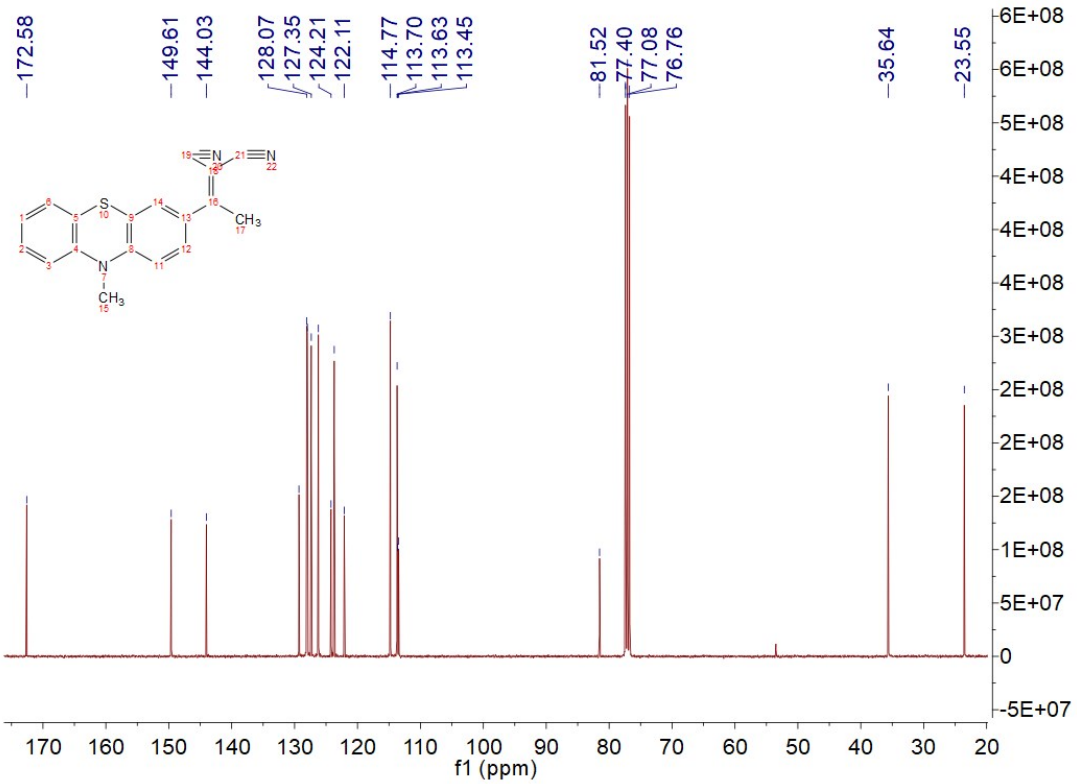

Fig. S26. ^{1}H NMR spectrum of **PTZ-3** in $CDCl_3$.

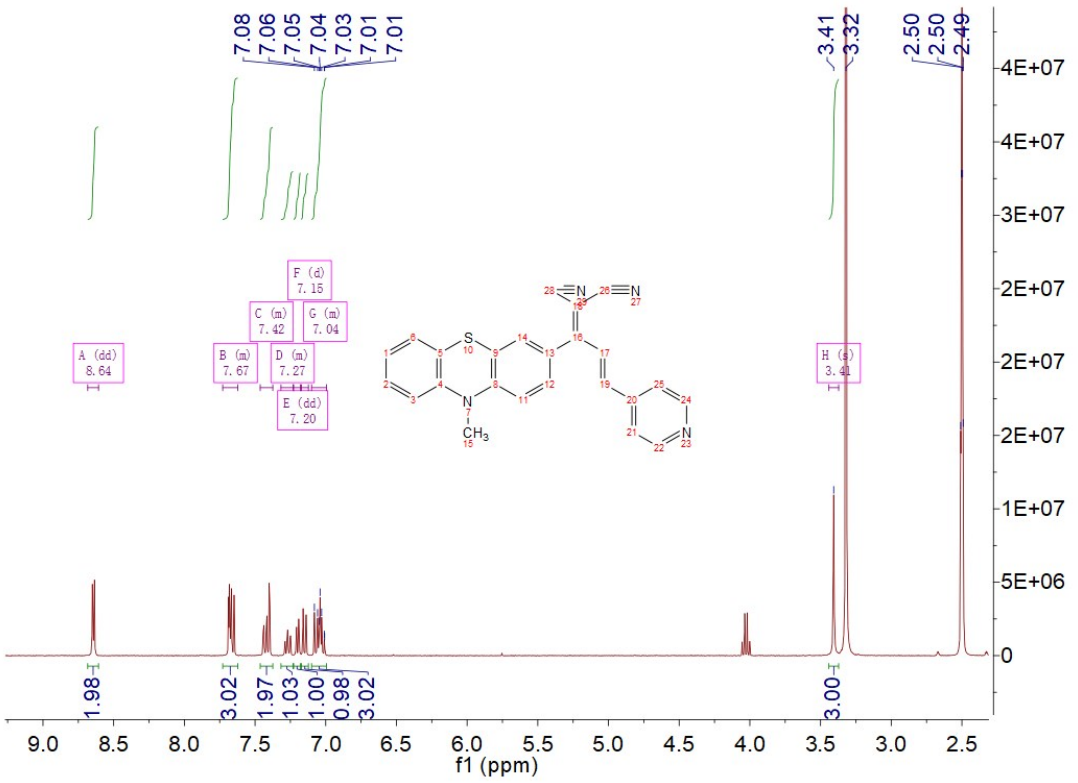

Fig. S27. ^{1}H NMR spectrum of **NPTZ-P1** in DMSO.

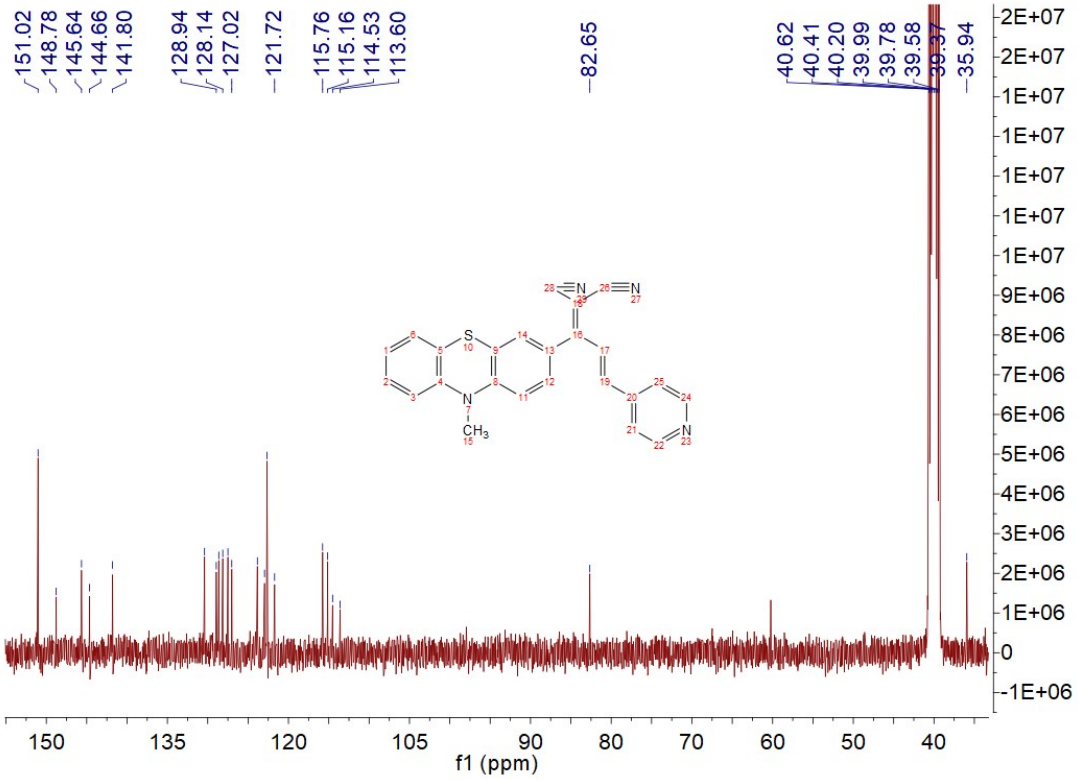

Fig. S28. ^{13}C NMR spectrum of **NPTZ-P1** in DMSO.

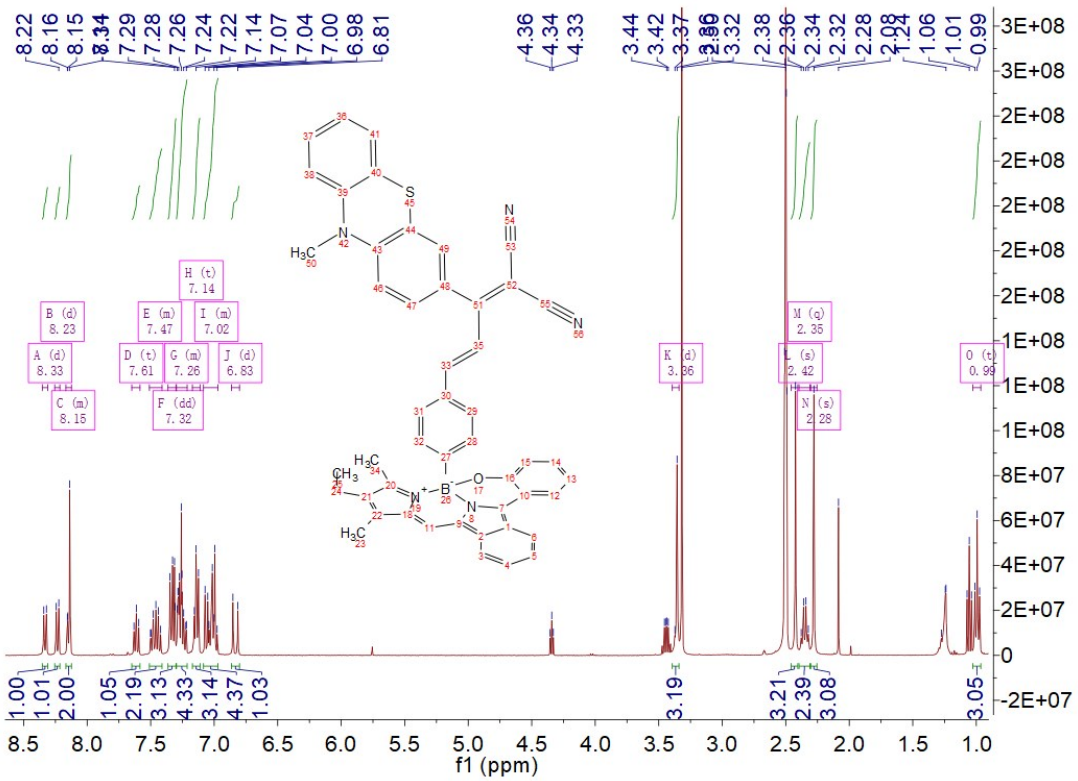

Fig. S29. ^{1}H NMR spectrum of **NPTZ-P2** in DMSO.

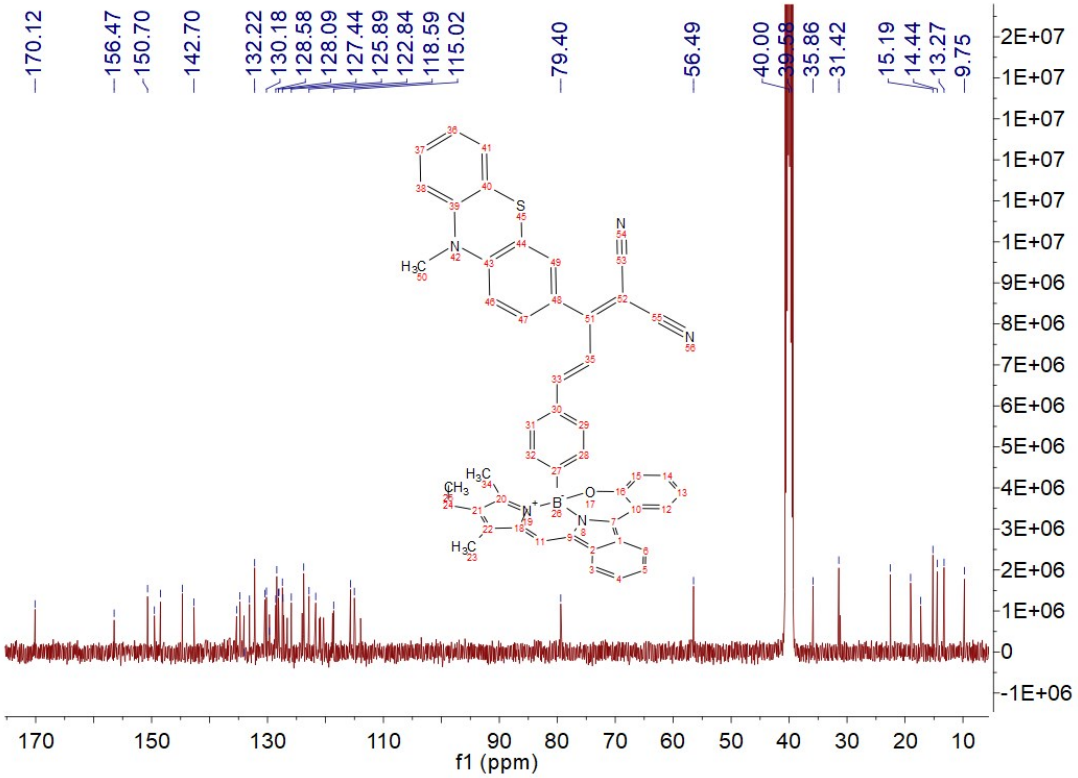

Fig. S30. ^{13}C NMR spectrum of **NPTZ-P2** in DMSO.

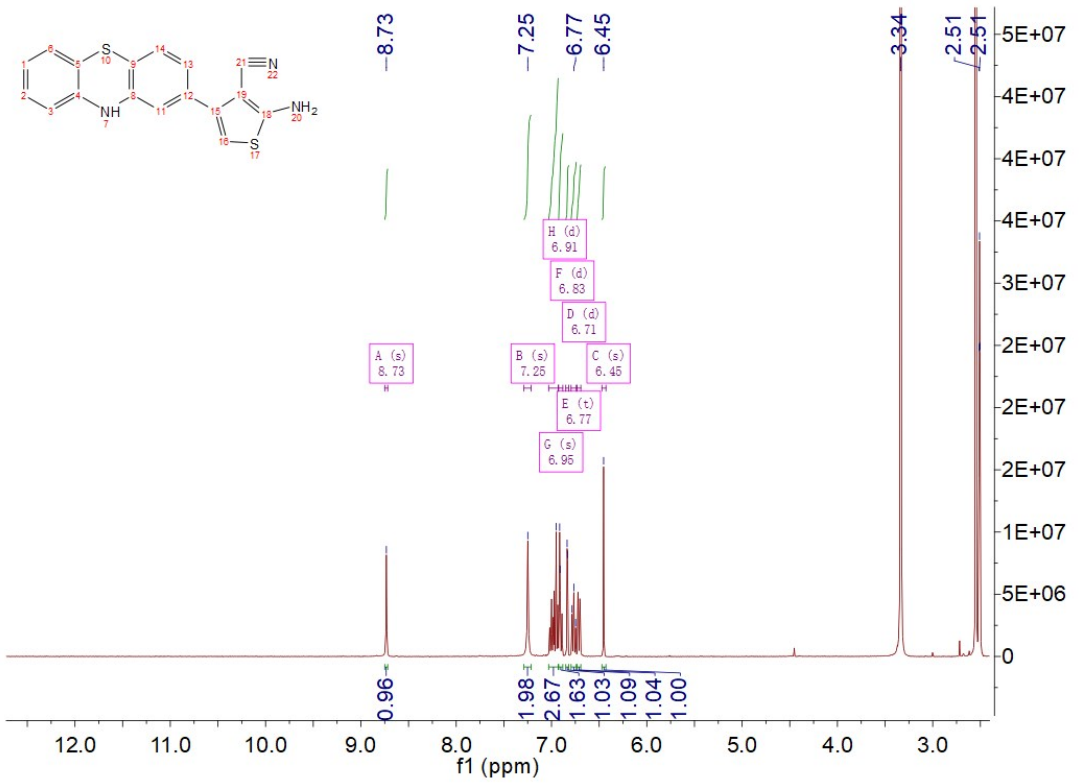

Fig. S31. ^{1}H NMR spectrum of **SF1** in DMSO.

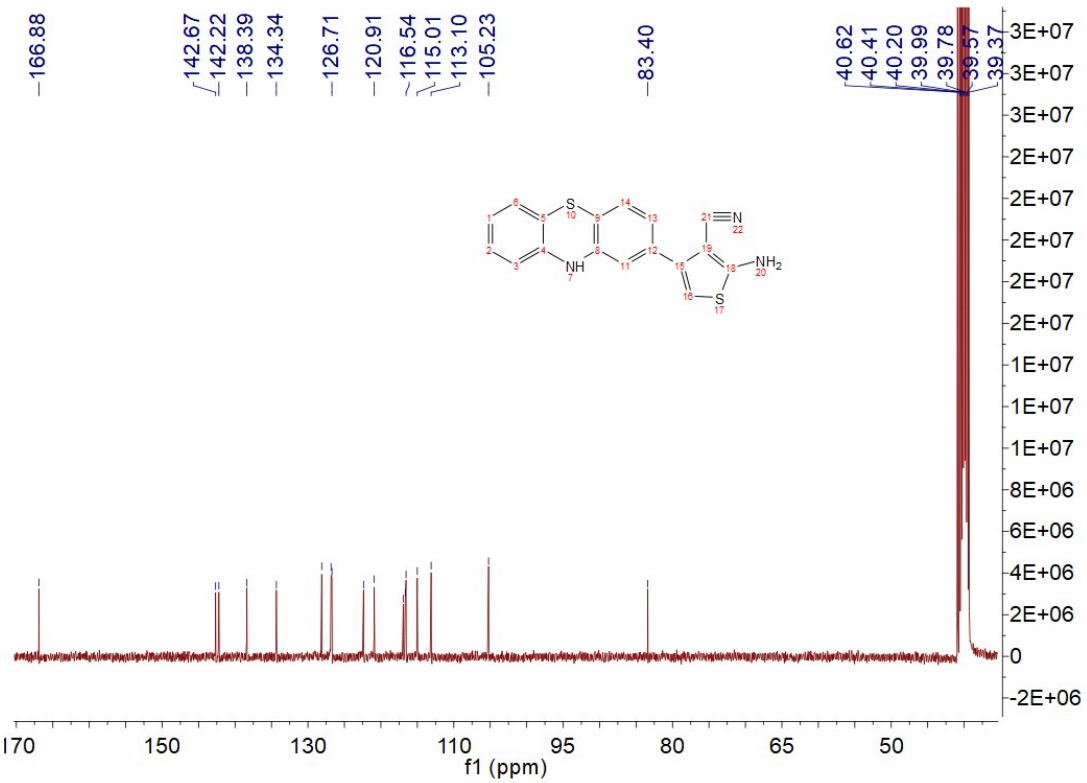

Fig. S32. ^{13}C NMR spectrum of **SF1** in DMSO.

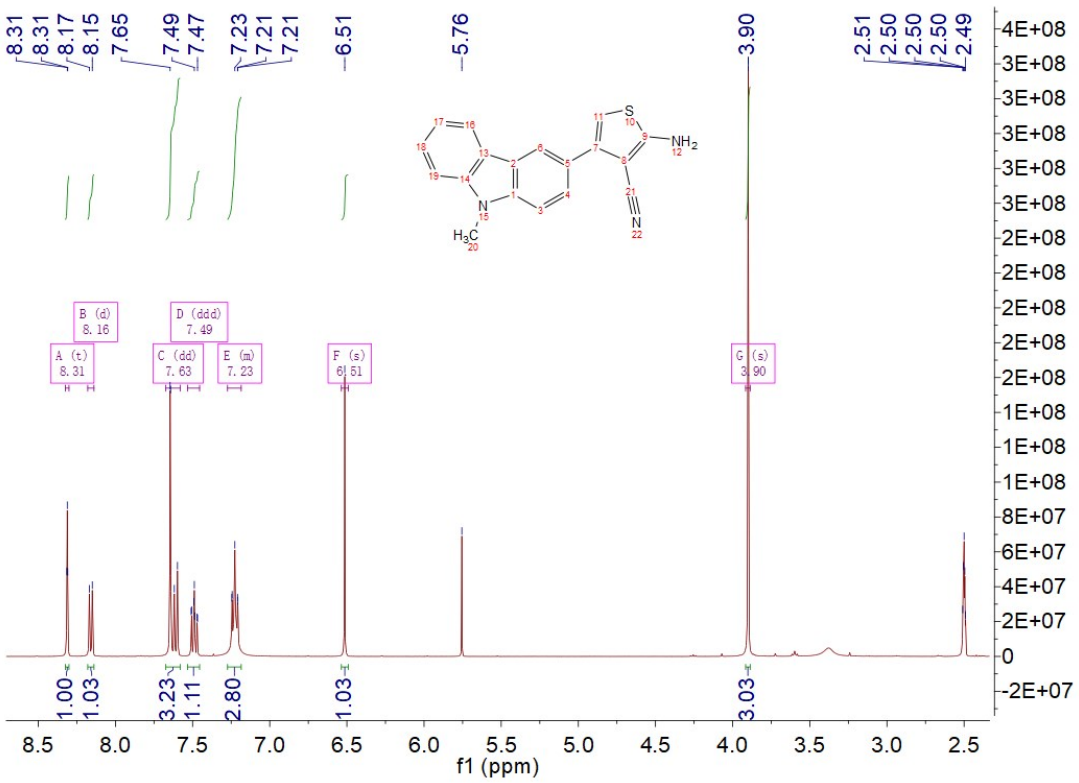

Fig. S33. ^{1}H NMR spectrum of **SF2** in DMSO.

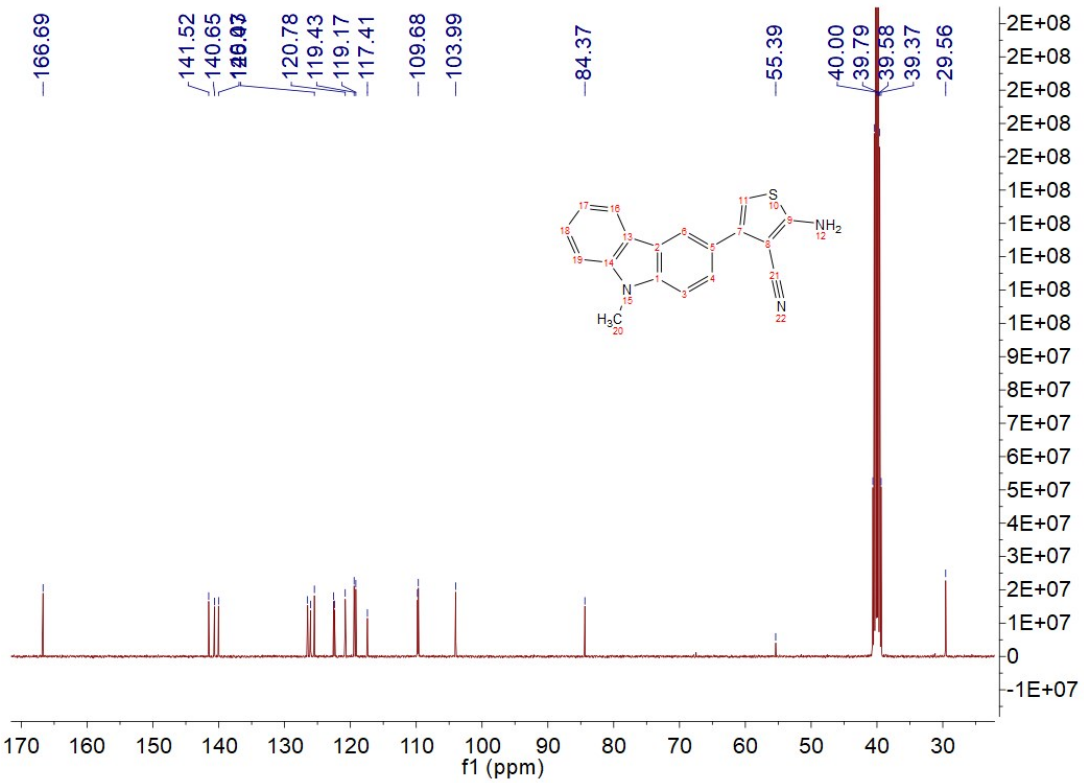

Fig. S34. ^{13}C NMR spectrum of **SF2** in DMSO.

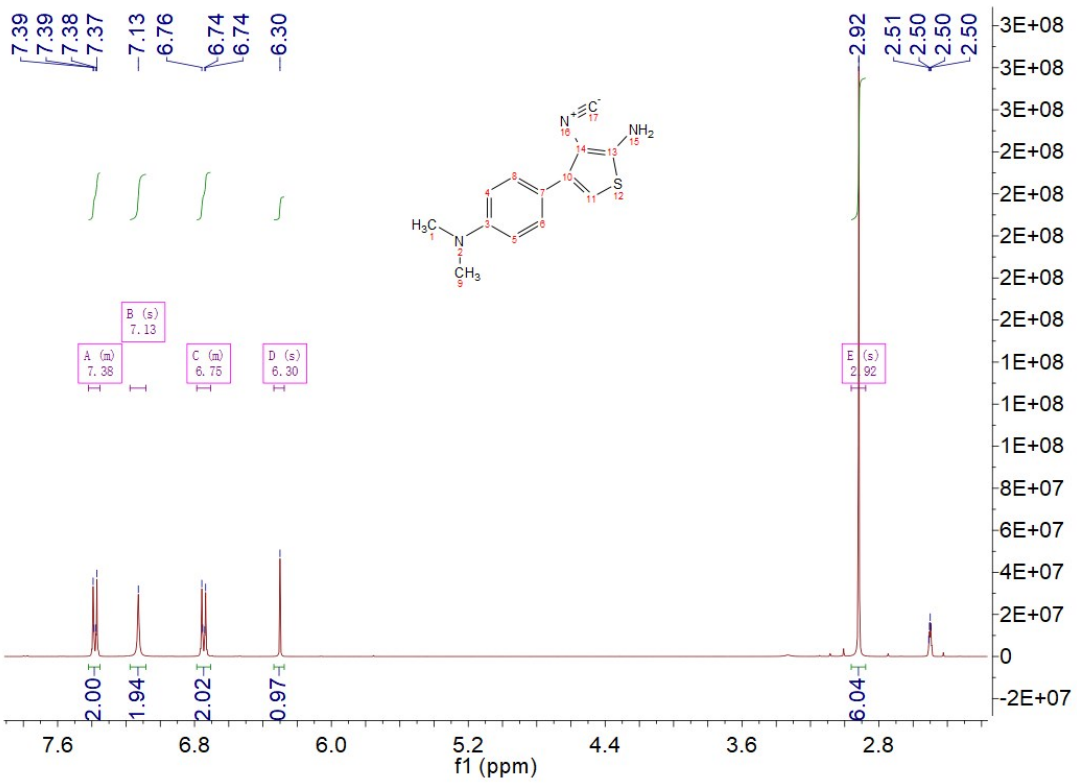

Fig. S35. ^{1}H NMR spectrum of **SF3** in DMSO.

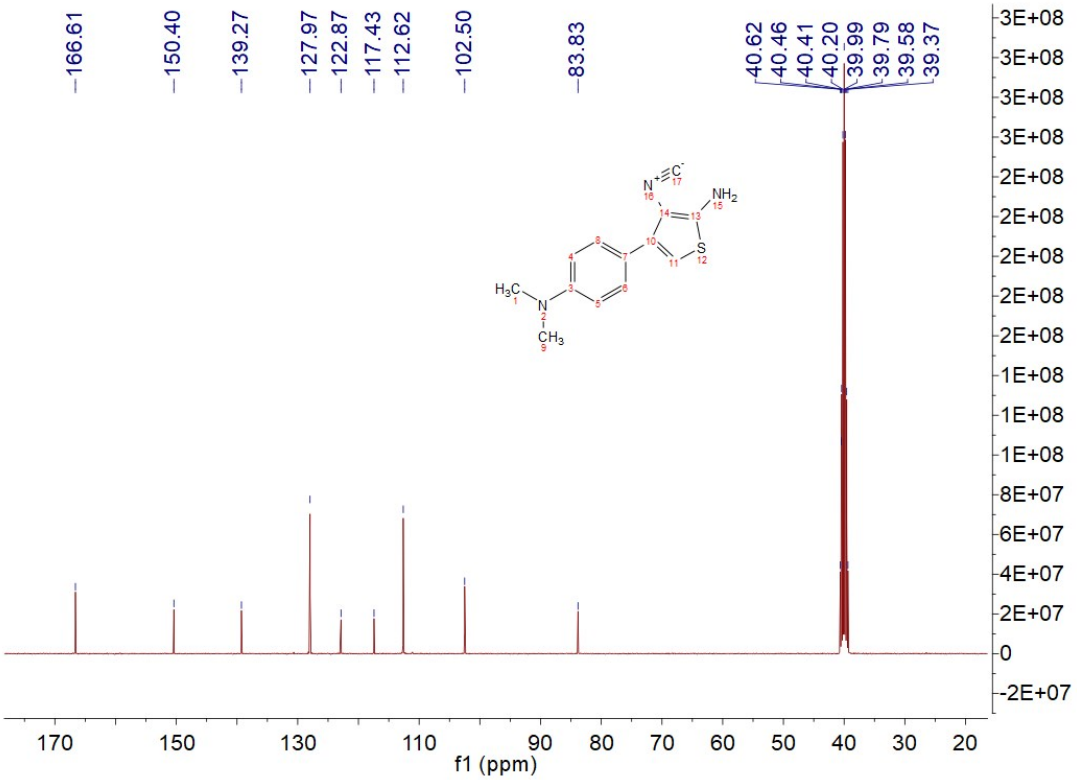

Fig. S36. ^{13}C NMR spectrum of **SF3** in DMSO.

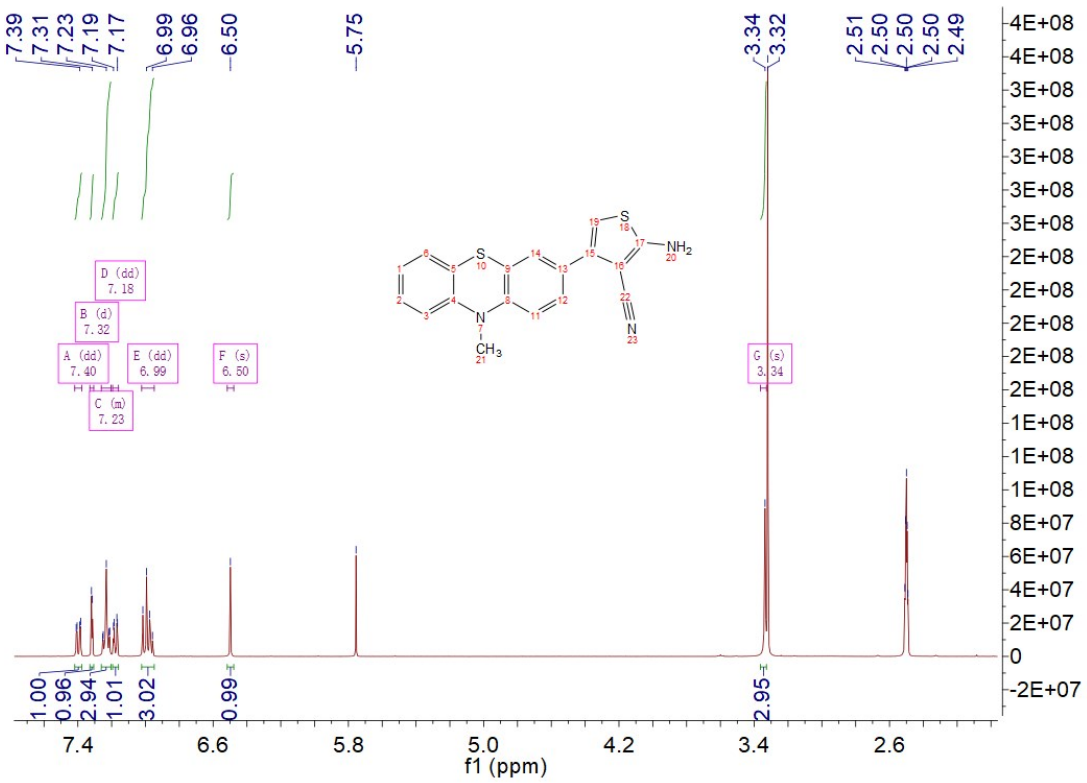

Fig. S37. ^{1}H NMR spectrum of **SF4** in DMSO.

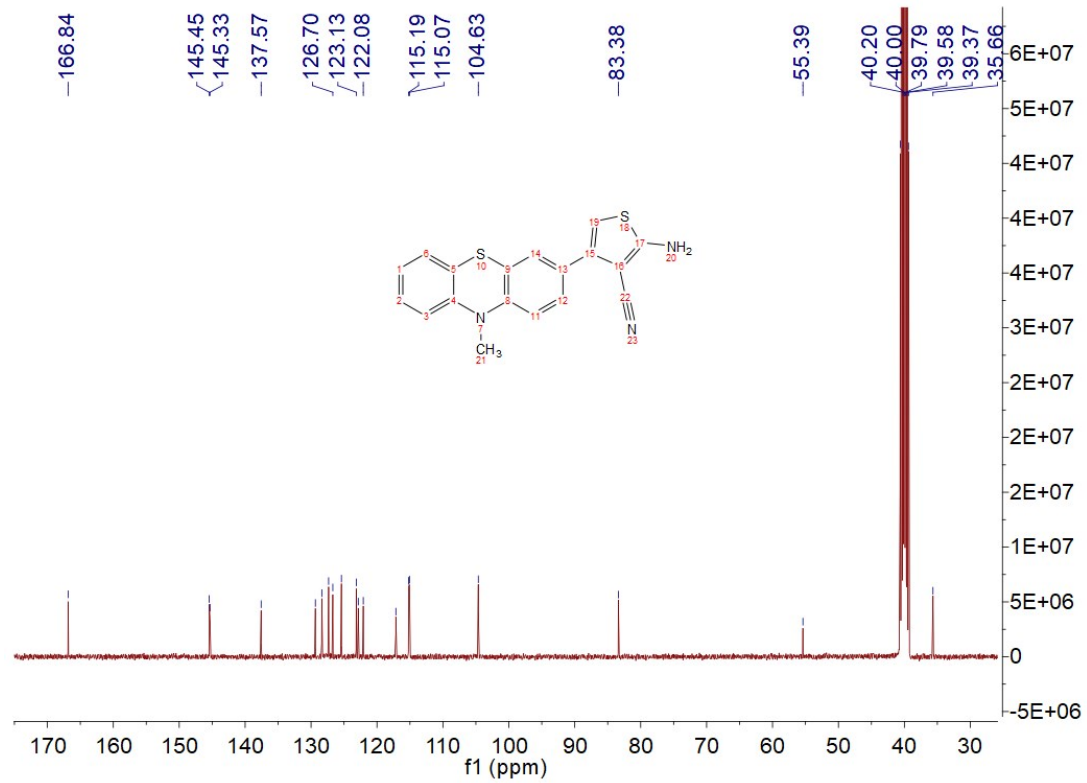

Fig. S38. ^{13}C NMR spectrum of **SF4** in DMSO.

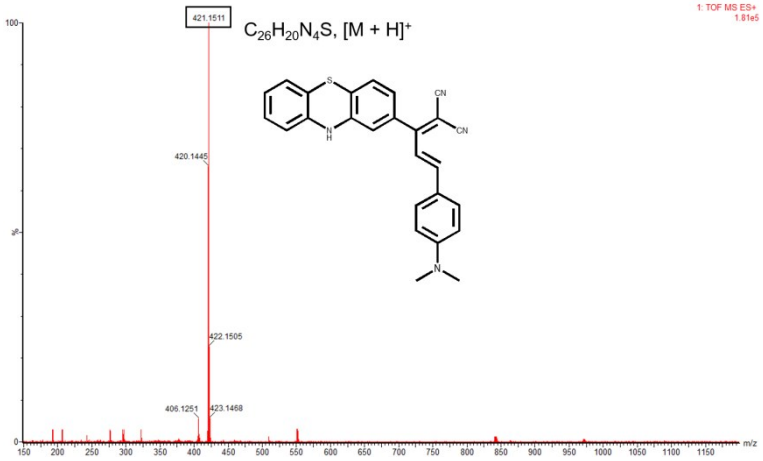

Fig. S39. HRMS spectra of **PTZ-P1**.

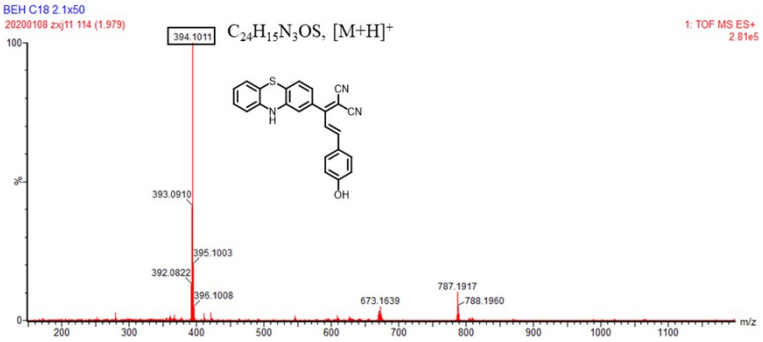

Fig. S40. HRMS spectra of **PTZ-P2**.

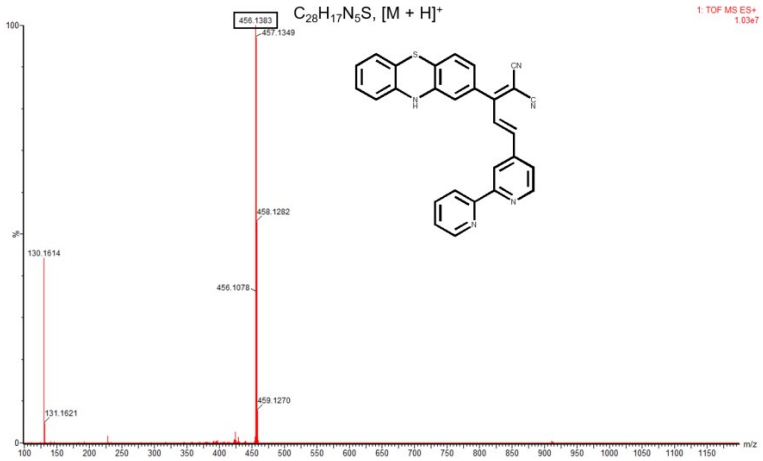

Fig. S41. HRMS spectra of **PTZ-P4**.

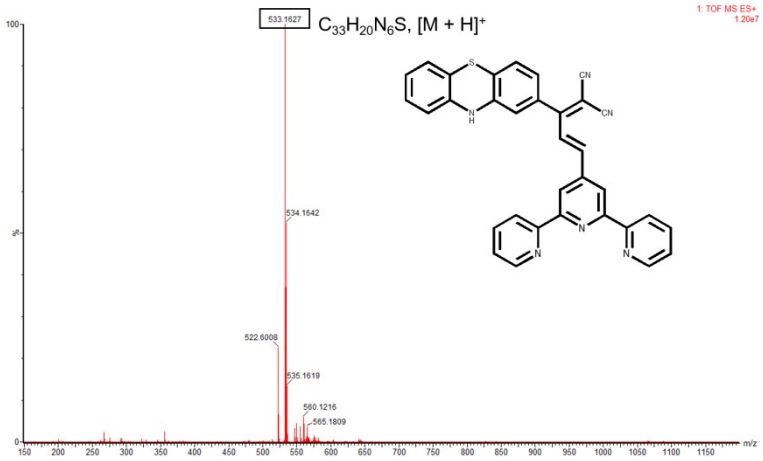

Fig. S42. HRMS spectra of **PTZ-P5**.

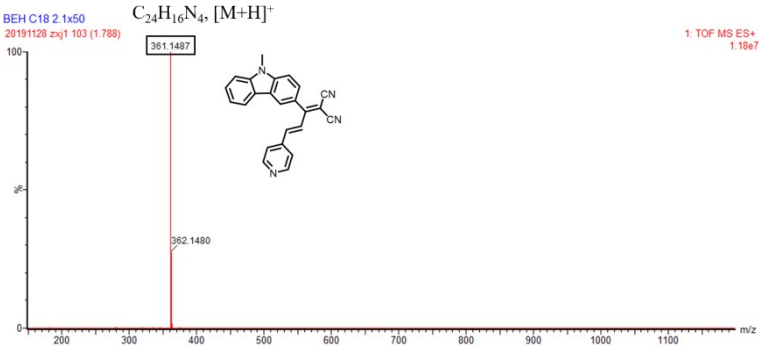

Fig. S43. HRMS spectra of **KZ-P**.

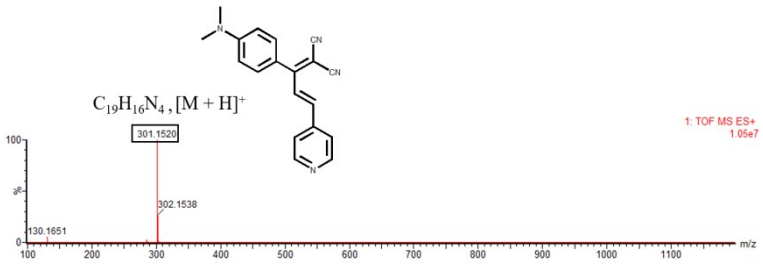

Fig. S44. HRMS spectra of **NNP-P**.

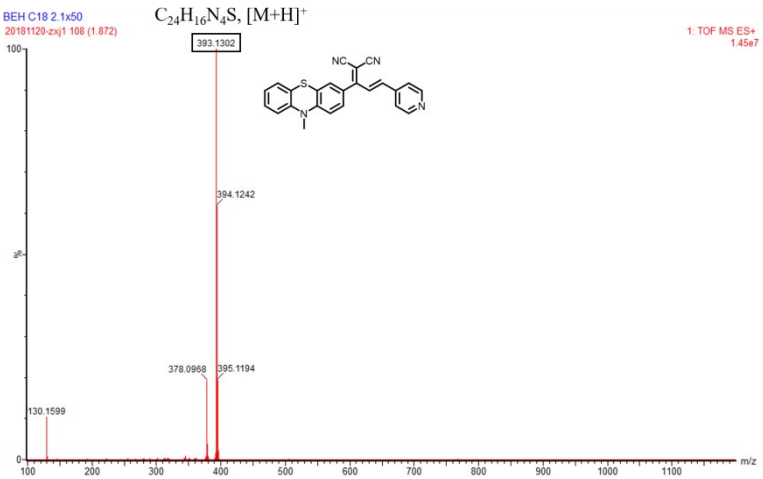

Fig. S45. HRMS spectra of **NPTZ-P1**.

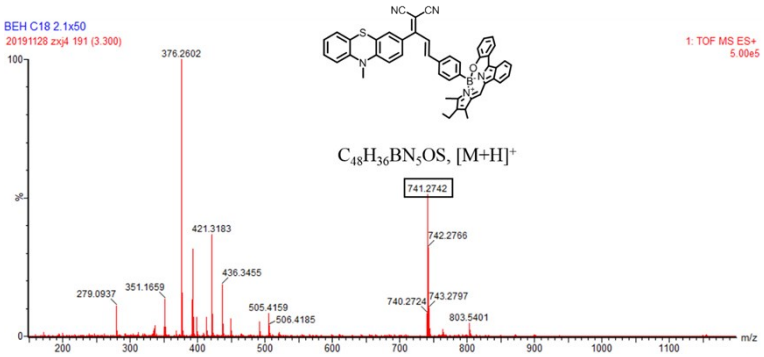

Fig. S46. HRMS spectra of **NPTZ-P2**.

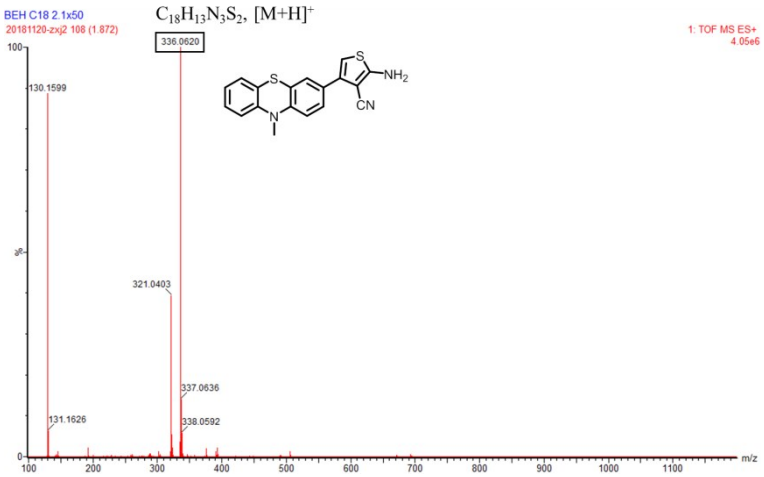

Fig. S47. HRMS spectra of **SF4**.

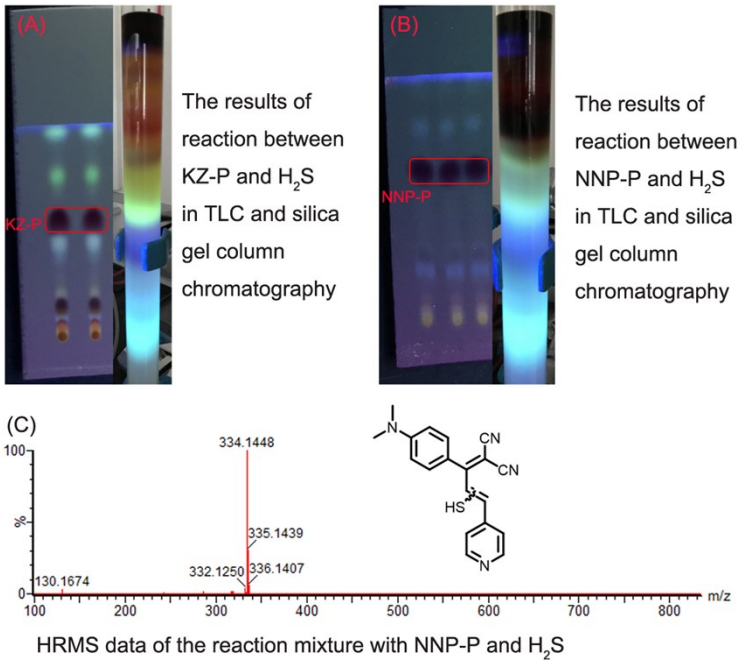

Fig. S48. The results of KZ-P and NNP-P reacted with H_2S.

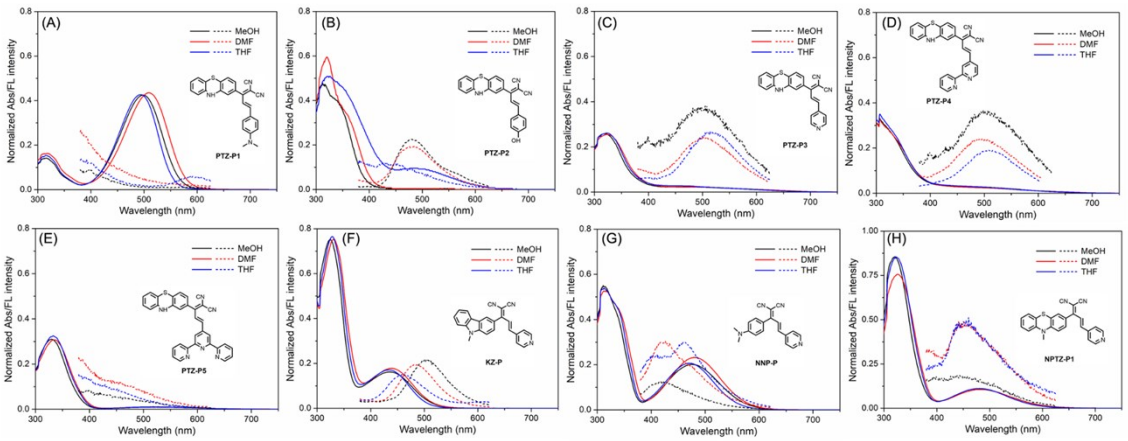

Fig. S49. Absorption and fluorescent spectra of probes (10 μM, **PTZ-P1**, **PTZ-P2**, **PTZ-P3**, **PTZ-P4**, **PTZ-P5**, **KZ-P**, **NNP-P** and **NPTZ-P1**) in different solvents (MeOH, DMF and THF), λ_{ex}=330 nm. Full lines and dotted lines represent absorption and fluorescent spectra respectively.

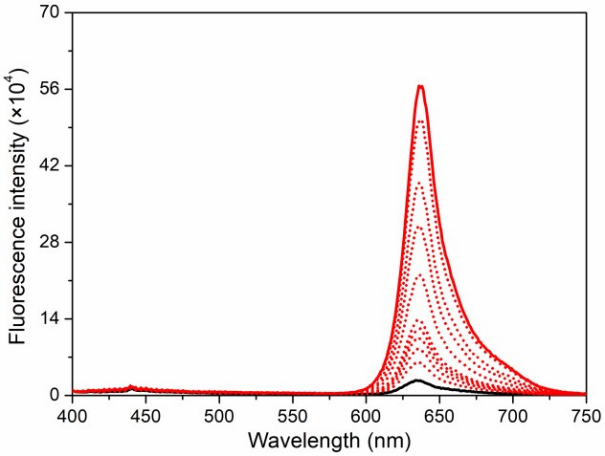

Fig. S50. Fluorescent spectra of **NPTZ-P2** (10 μM) in PBS buffer (pH=7.4)/DMSO (1/2, 2% v/v PEG 400) with addition of H_2S (0-600 μM), λ_{ex}=390 nm.

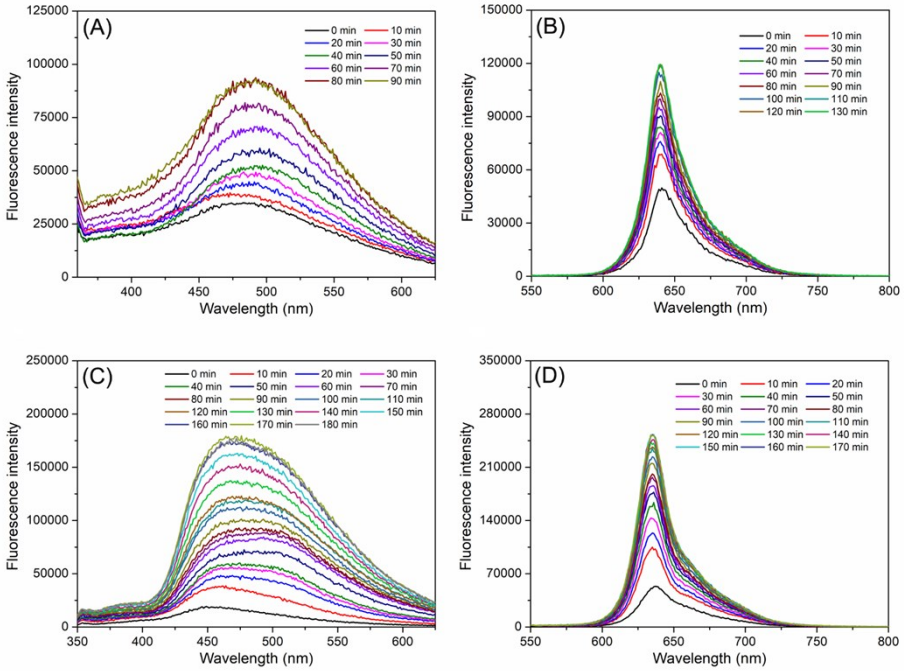

Fig. S51. Time-dependent fluorescence intensity changes of **PTZ-P1** (A), **PTZ-P6** (B), **NPTZ-P1** (C) and **NPTZ-P2** (D) (10 μm) with H_2S (100 μm) in PBS buffer (pH=7.4)/DMSO (1/2 v/v, 2% PEG 400).

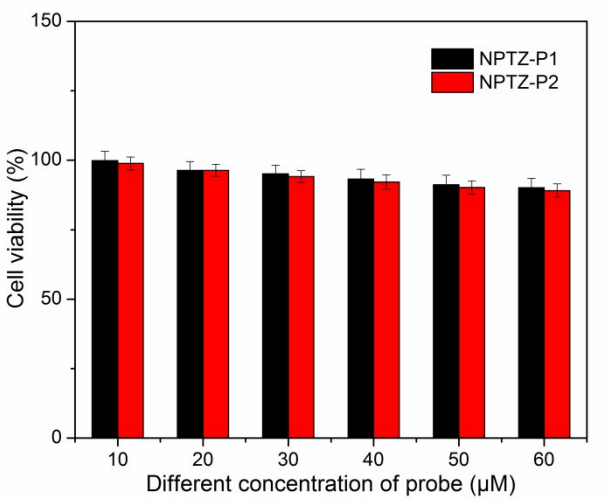

Fig. S52. Viabilities of HeLa cells after incubation with different concentrations of **NPTZ-P1** and **NPTZ-P2** for 24 h.

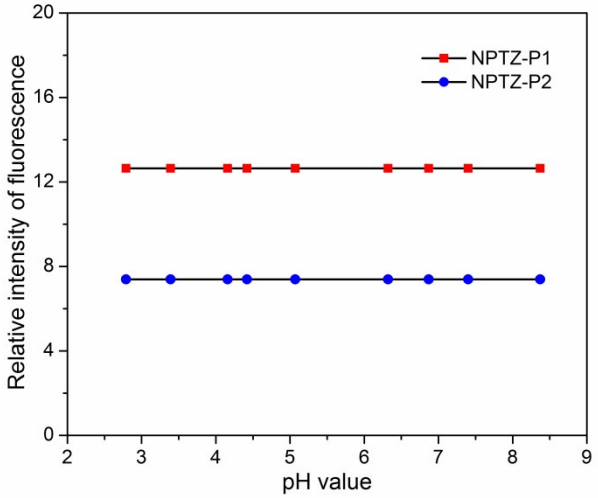

Fig. S53. The fluorescence emission changes with the pH titration curve of 10 μM **NPTZ-P1** (λ_{ex}=330 nm, λ_{ex}=455 nm) and **NPTZ-P2** (λ_{ex}=550 nm, λ_{ex}= 635 nm), pH value: 2.79, 3.39, 4.16, 4.42, 5.07, 6.32, 6.87, 7.4, 8.37 (from left to right).

Table S1. Calculated linear absorption properties (nm), excitation energy (eV), oscillator strengths and major contribution for selected compounds

Compounds	Energy Gap (eV)	λ (nm)	*f*	Composition	HOMO (eV)	LUMO (eV)
PTZ-P1	2.2110	560.75	0.0593	HOMO→LUMO (0.70057)	-5.15	-2.50
PTZ-P2	2.0484	605.27	0.0540	HOMO→LUMO (0.70402)	-5.29	-2.81
PTZ-P3	1.8044	687.11	0.0510	HOMO→LUMO (0.70478)	-5.46	-3.23
PTZ-P4	1.8230	680.12	0.0559	HOMO→LUMO (0.70467)	-5.44	-3.21
PTZ-P5	1.8382	674.48	0.0544	HOMO→LUMO (0.70453)	-5.37	-3.11
KZ-P	2.5581	484.67	0.1602	HOMO→LUMO (0.6986)	-5.90	-2.99
NNP-P	2.5643	483.51	0.2353	HOMO→LUMO (0.7009)	-5.71	-2.86
NPTZ-P1	2.1084	588.06	0.1427	HOMO→LUMO (0.70328)	-5.57	-3.11